

# Dynamics and vibration of a 3-PSP parallel robot with flexible moving platform

Mahdi Sharifnia and Alireza Akbarzadeh

Journal of Vibration and Control  
2016, Vol. 22(4) 1095–1116  
© The Author(s) 2014  
Reprints and permissions:  
sagepub.co.uk/journalsPermissions.nav  
DOI: 10.1177/1077546314538882  
jvc.sagepub.com



## Abstract

In this research, first an analytical model is presented for dynamic and vibration analysis of a 3-PSP parallel robot with a flexible moving platform. Next, the presented analytical model is solved using an approximate analytical method. The moving platform is assumed to be made of three Euler-Bernoulli beams joined together to form a star. Each of the three beams of the star slides through a passive prismatic joint. Then, three-dimensional vibration analysis of the flexible moving platform, star, with three passive prismatic joints is the main subject of the present research. Only vibration during free motion is considered. Therefore, it is assumed that only inertia forces of the star are the main source of its vibration. First, direct kinematics is used for acceleration analysis of the rigid robot and inertia forces are obtained. For dynamic modeling, the passive prismatic joints and junction point of the three beams are modeled using a new set of geometric constraints. Additionally, a previously developed constrained motion equation for a planar Euler-Bernoulli beam having a prismatic joint is further developed for the three beams of the star. Next, an approximate analytical solution method, called the “constrained assumed modes method”, is used for inverse dynamics and vibration analysis of the robot. Furthermore, the developed model can be used for direct dynamics analysis of the robot. Finally, several input trajectories and two different groups of mode shapes are considered to investigate the model efficiency. The results of the presented model are compared with the results of a commercial finite element method software.

## Keywords

Assumed modes, flexible, parallel robot, prismatic joint, vibration

## 1. Introduction

This research involves two main research areas such as flexible multi-body dynamics and parallel manipulators. High speed and accuracy together with high stiffness to weight ratio are reasons why parallel robots are an important part of industrial applications. Microsurgery, space robotics, maintenance of nuclear plants and high speed pick and place tasks represent some of the applications commonly used by the parallel robots. On the other hand, decreasing robot weight enables additional potential applications. However, parallel robots constructed with lightweight materials can result in undesirable vibration. In these cases, selected modeling methods in flexible multi-body dynamics may be used to obtain a vibrational response. Parallel robots commonly have many passive joints which increase the number of kinematic constraints. Therefore, constrained flexible multi-body dynamics is a more specific area that can be used in the analysis of flexible parallel robots. In this research, we present the

vibration analysis of a spatial parallel robot called 3-PSP where its flexible moving platform has three passive prismatic joints.

Flexible multi-body dynamics have been studied by many researchers. Common global methods to describe flexibility of the structures are lumped parameter modeling, finite element method (FEM) and assumed mode method (AMM). Perhaps the most used method in flexible multi-body dynamics is the floating frame of reference formulation based on the FEM. This method was introduced by Song and Haug (1980) and extended by

---

Center of Excellence on Soft Computing and Intelligent Information Processing (SCIIP), Mechanical Engineering Department, Ferdowsi University of Mashhad, Iran

Received: 24 January 2014; accepted: 4 May 2014

### Corresponding author:

Mahdi Sharifnia, Center of Excellence on Soft Computing and Intelligent Information Processing (SCIIP), Mechanical Engineering Department, Ferdowsi University of Mashhad, Mashhad 0098, Islamic Republic of Iran.  
Email: sharifnia.mehdi@gmail.com

Shabana and Wehage (1983). Also, Yoo and Haug (1986a,b) introduced a method based on the FEM using vibration and static correction modes. The AMM may need to use a large number of mode shapes to successfully model kinematic joints, for example translational joints, with concentrated loads. Consequently, this approximate analytical method or other analytical methods are less extended to vibration analysis of flexible parallel robots.

Many studies have presented the motion of a flexible beam with prismatic joint. For example, Tabarrok et al. (1974), Banerjee and Kane (1987), Wang and Wei (1987), Yuh et al. (1989), Krishnamurthy (1989), Theodore and Ghosal (1997) and Gurgoze and Yuksel (1999) used AMM to study vibration analysis of an axially moving beam with prismatic joint. Additionally, Stylianou and Tabarrok (1994) and Lee and Jang (2007) used FEM. Some of these researchers applied their model to flexible cylindrical (Krishnamurthy, 1989) or spherical (Theodore and Ghosal, 1997) manipulators. Additionally, the study of flexible beams can be extended to vibration analysis of flexible robots (Sharifnia and Akbarzadeh, 2014a).

Many researchers have used FEM for vibration analysis of flexible parallel robots. Fattah et al. (1994a,b, 1995) used the potential energy of a beam element in their FEM model to describe flexibility of a “planar beam-shaped flexible link”. They presented kinematics and dynamics of a flexible 3-RRS parallel robot. Piras et al. (2005) presented a dynamic finite element analysis for a flexible planar 3-PRR parallel robot. They investigated the effect of high-speed motions and configuration of the mechanism on the vibrations of the robot. Using the Lagrange finite element model for flexible linkages, Wang and Mills (2006) presented substructuring dynamic modeling for a flexible-link planar 3-PRR parallel robot. Some researchers used approximate analytical methods for vibration analysis and active control of flexible parallel robots. Kang and Mills (2002) and Zhang et al. (2008) presented an analytical model for a flexible planar 3-PRR parallel robot using AMM and Lagrange’s multipliers.

In general, dynamic modeling of flexible parallel robots with translational joints is relatively complicated. The translational joints create time-variant boundary conditions or holonomic constraints on the flexible links. On the other hand, generalized coordinates used in the dynamic modeling can create complexities in the joint constraint equations and nonlinearity in the motion equations (Sugiyama et al., 2003). When a body coordinate system and an elastic coordinate system are used for the dynamic modeling of a prismatic joint, depending on the modeling procedure and interference of these two coordinate systems, geometric nonlinearities can appear in the motion

equations (Sharifnia and Akbarzadeh, 2014a). In previous work, modal coordinates have mostly been preferred when the vibrational problems with time-invariant boundary conditions have been studied. To the best of the authors’ knowledge, aside from a few FEM studies, there exist only two approximate analytical studies on vibration analysis of flexible parallel robots with passive prismatic joints (Sharifnia and Akbarzadeh, 2014a,b). Sharifnia and Akbarzadeh (2014a), authors of the present paper, developed a motion equation in variational form for vibration and control analysis of a Euler-Bernoulli beam with a passive prismatic joint. A flexible beam with a general planar motion is used as a moving platform of a PR-PRP parallel robot. Sharifnia and Akbarzadeh (2014b) presented vibration analysis of a planar 3-PRP parallel robot called ST (Star-Triangle). The robot has a flexible moving platform with three passive prismatic joints. The authors used a constrained assumed modes method (Camm) for vibration analysis of the PR-PRP and the 3-PRP parallel robots. As presented by Sharifnia and Akbarzadeh (2014a,b), there is a difference between the AMM and Camm. In the assumed modes method, each of the assumed mode shapes must satisfy all the geometrical boundary conditions. However, using the constrained assumed modes method, the assumed mode shapes each satisfies only time-invariant geometrical boundary conditions and do not satisfy time-variant geometrical boundary conditions. Instead, by writing additional time-variant constraint equations, the combination of the assumed modes will satisfy the time-variant geometrical boundary conditions. In other words, this method applies the time-variant constraints of the prismatic joint on the assumed modes method (Sharifnia and Akbarzadeh, 2014b). Ibrahimbegovic and Mamouri (2000) presented a finite element implementation of the internal constraints in a three-dimensional exact beam model. Bauchau (2000) presented FEM modeling of prismatic joints in the flexible multi-body systems. This reference demonstrated different behavior of prismatic and sliding joints. Including the passive prismatic joint parameters such as mass, moment of inertia and its actual length increases the challenges for dynamic modeling of the flexible parallel robots (Sharifnia and Akbarzadeh, 2014b). For rigid planar kinematic chains, Stoenescu and Marghitu (2004) showed that the moment of inertia of the prismatic joints has significant effects at high speeds. Sharifnia and Akbarzadeh (2014a) investigated the effects of the actual prismatic joint length on the vibrational behavior of the PR-PRP parallel robot.

Considering the existing body of literature on flexible parallel manipulators, it may be concluded that (1) Analytical methods are less used and most researchers

used FEM or other numerical methods for the vibration analysis of parallel robots; (2) There are few existing FEM studies on flexible parallel robots with prismatic joints. There are only two existing approximate analytical studies where the moving platform is flexible and has passive prismatic joint; (3) The effect of mass, moment of inertia and actual length of the prismatic joint on the vibration response is considered less in the analytical methods.

The present study aims to offer certain advantages for each of the above three shortcomings. To do this, a spatial 3-PSP parallel robot (Rezaei et al., 2012, 2013) having a flexible moving platform and three passive prismatic joints is considered. The 3-PSP parallel robot presented in this research has three symmetric closed loop chains. Each chain consists of an active prismatic joint (P), a passive spherical joint (S) and a passive prismatic joint (P).

In this paper, the authors intend to further develop their previous modeling and solution method and to obtain more accurate results. To do this, a new set of geometric constraints for dynamic modeling of the passive prismatic joints as well as a new set of geometric constraints for the junction point of the three beams of the flexible moving platform are presented for a more complicated spatial 3-PSP robot.

The rest of this paper is organized as follows. In Section 2, Robot structure and assumptions are introduced. In Section 3, Direct kinematics of the robot is presented. In Section 4, New constraint equations for

the center of the moving platform, star, are developed. In Section 5, Motion equations and new constraints for modeling of the prismatic joints are developed, and the motion constraints are incorporated into the motion equation. In Section 6, An approximate analytical solution for the motion equations using the “constrained assumed modes method” is presented. In Section 7, Numerical results of three case studies are presented. In Section 8, A short discussion about mode shape selection and its effect on the accuracy of the approximate analytical solution is presented, and in Section 9, Concluding remarks are presented.

## 2. Robot structure and assumptions

The 3-PSP robot is a fully parallel robot with three degrees of freedom (d.f.). Several types of 3-PSP parallel robot can be assembled. Structures of the 3-PSP robot, solid and experimental models, used in the present research are shown in Figure 1. In this structure, the moving platform is made of three flexible beams shaped like a star. Each of the three legs begins with an active prismatic joint (P) actuated by a linear rod in the Z-direction, a passive spherical joint (S) and a passive prismatic joint (P), which slides through one of three beams of the star. The three beams have the same physical and geometrical properties and the plane and angle between each two branches of the star is 120 degrees. Finally, the three linear actuator rods are aligned vertically on three

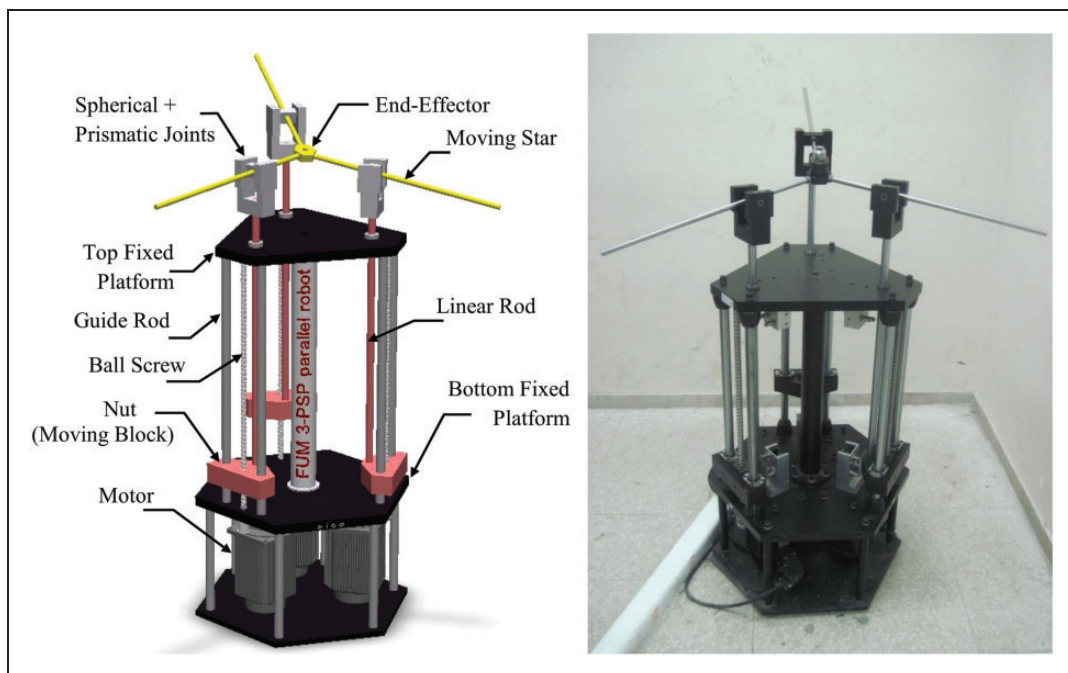


Figure 1. Solid and physical model of the 3-PSP parallel robot.

corners of an equilateral triangle (fixed triangular base of the robot).

In the present research for dynamic modeling of the 3-PSP robot, the three branches of the moving star, also referred to as beams 1, 2 and 3, are each considered as a discrete Euler-Bernoulli beam with a prismatic joint. The rigid configuration of the star is called the rigid star and a plane obtained from three beams of the rigid star is called “rigid star plane”. Consider Figure 2, which shows coordinate systems used on the 3-PSP robot. Points  $I$ ,  $J$  and  $K$  represent centers of the three passive prismatic joints. Points  $A$ ,  $B$  and  $C$  represent three ends of the beams 1, 2 and 3, respectively. As shown, a fixed coordinate system  $XYZ$  with its origin attached to point  $O$  at the center of the fixed triangular base is defined. A rigid body coordinate system  $xyz$  is attached to point  $G$ , end-effector, for the star. Its  $y$ -axis is in the opposite direction of vector  $\overrightarrow{GI}$  and its  $z$ -axis is in the same direction as the normal vector of the rigid star plane. At the start of motion, the  $z$  and  $Z$ -axis are collinear and the  $x$  and  $y$ -axis are parallel with the  $X$  and  $Y$ -axis, respectively. Additionally, at the start of motion, the velocity of each of the input trajectories is assumed to be zero and the robot has no elastic deformation. Finally, at the start of motion, each of the three beams of the star is perpendicular to the corresponding rigid link (linear rod) of the robot.

At rigid and deformed configurations, the center of the moving star is called  $G$  and  $G'$ , respectively. During the motion analysis, the deformed configuration of the star is measured with respect to the rigid body coordinates attached to the rigid configuration of the star. As stated earlier, the rigid body coordinate system  $xyz$  is attached to the rigid configuration of the star. Next, for the beams 1, 2 and 3, three additional rigid body coordinate systems are considered as  $x_1y_1z_1$ ,  $x_2y_2z_2$  and  $x_3y_3z_3$ , respectively. The three rigid body coordinate systems are each attached to the rigid configuration of the corresponding beam. Their origins are located at the midpoint of the corresponding rigid beam. The direction for each of the  $x_i$ -axis is along the axis of the rigid beam  $i$  and passes through the center of the passive prismatic joint. The direction for each of the  $z_i$ -axis is normal to the rigid star plane. Elastic displacements in the directions of  $x_i$ ,  $y_i$  and  $z_i$  axes are denoted by  $u_i$ ,  $v_i$  and  $w_i$ , respectively. Finally, it is assumed that input trajectories of the actuators in the  $Z$ -direction are entirely transferred to them without any error.

Each of the three beams of the star can vibrate in two transverse directions,  $y_i$  and  $z_i$ . The elastic displacement  $v_i$  takes place in the rigid star plane and the elastic displacement  $w_i$  takes place out of the rigid star plane. In this paper, we refer to  $v_i$  and  $w_i$  as in-plane and out-of-plane transverse vibrations, respectively.

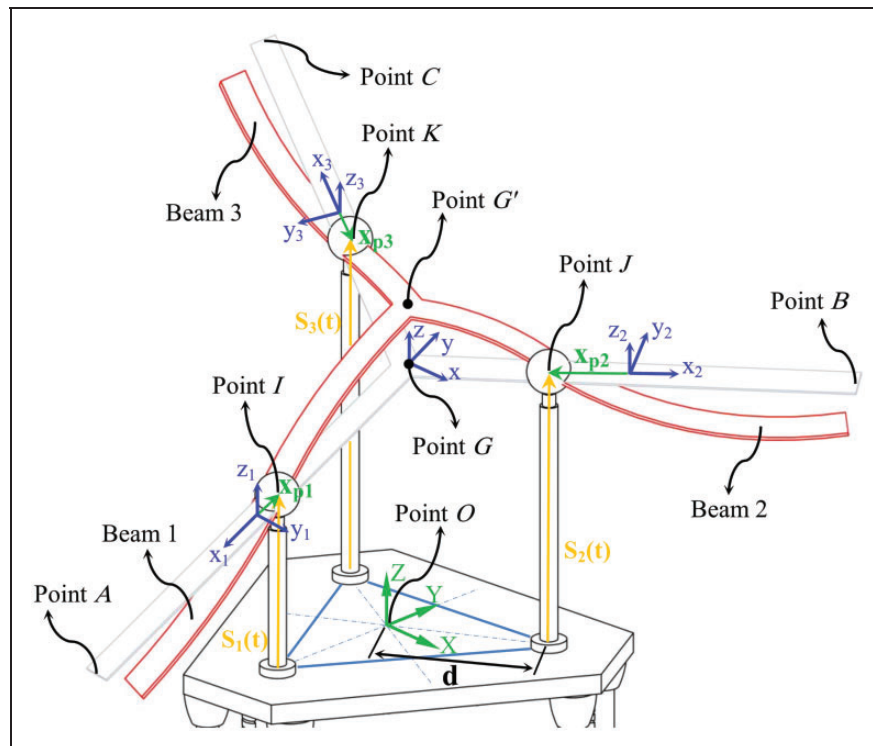


Figure 2. Fixed and rigid body coordinate systems of the 3-PSP robot.

The in-plane transverse vibration is normal to the beam axis and lies in the rigid star plane. The out-of-plane transverse vibration is normal to the rigid star plane. For simplification, it is assumed that in-plane bending stiffness for three beams of the star is much higher (about 100 times) than out-of-plane bending stiffness and consequently in-plane transverse vibration for the three beams is neglected. Therefore, vibration is only in the  $w_i$ -direction. Note that because in-plane bending stiffness is assumed to be much higher than out-of-plane bending stiffness, torsional stiffness is also much higher (about 50 times) than out-of-plane bending stiffness. Additionally, because the prismatic joint is located within a spherical joint, one end of the beam is free to rotate about  $x_i$  axis and does not experience any twist load. Therefore, torsional vibration and its effects on the elastic displacement of the beams are also neglected. Finally, in order to focus on off-load behavior of the robot, concentrated inertia or external load are not added to the robot's end-effector. Because each branch of the moving platform is assumed to be a Euler-Bernoulli beam, the effects of shear deformation and rotational inertia moment are not considered in dynamic modeling. The magnitude and the slope angle of the beam deformation are also assumed to be small (see theory of Euler-Bernoulli beam).

Additional assumptions are obtained from the main purpose of this paper, which is to develop a dynamic model for the robot to be a ground for future works such as trajectory control. In this research, it is assumed that input trajectories of the active joints can be obtained without any significant error by the motor drive control system and consequently vibration of the 3-PSP robot at the points  $I$ ,  $J$  and  $K$  are assumed to be zero. Therefore, the rigid star is enforced to track the rigid configuration obtained from its three input trajectories. This assumption means that (a) it is the rigid body motion that induces the flexible body motion in the absence of initial conditions and external loads, and (b) that the flexible body motion does not affect the rigid body motion. Additionally, this assumption allows us to better see the behavior of the flexible body motion and verify the proposed model.

### 3. Direct kinematics of the 3-PSP robot

Initial conditions, external loads or inertia forces can cause a structure to vibrate. In this paper initial conditions and external loads are assumed to be zero and the agent of vibration is only inertia forces. Inertia forces appear in motion equations in terms of accelerations and velocities of the structure. Depending on the control strategies for a given motion, accelerations and velocities of rigid motion of a structure are directly calculated from either the direct or the inverse kinematics of the

assumed rigid structure which are next used in the dynamic motion equations of the flexible structure. They can also be indirectly entered in the motion equations by means of an energy method. In this section, using the direct kinematics of the 3-PSP robot, the required terms of accelerations and velocities of the rigid motion are calculated in order that they can be used in the motion equations of the flexible structure. Specifically, in the 3-PSP robot, acceleration and velocity for an element of the star are calculated from its rigid motion. Note that the acceleration term in the motion equation contains both rigid and flexible body accelerations. The rigid body motion induces the flexible body motion. By supplying the rigid body motion to the motion equations, the flexible body motion is obtained.

Given the trajectories of the actuated prismatic joints,  $s_1(t)$ ,  $s_2(t)$  and  $s_3(t)$ , the position trajectory of the working point of the robot, point  $G$ , as well as the normal vector to the rigid star plane must be determined. Consider Figure 2. Position vectors of the points  $I$ ,  $J$  and  $K$  in the fixed coordinate system  $XYZ$  are as follows:

$$\vec{OI} = \begin{bmatrix} 0 \\ -d \\ s_1(t) \end{bmatrix} \tag{1}$$

$$\vec{OJ} = \begin{bmatrix} +d \cos(\pi/6) \\ +d \sin(\pi/6) \\ s_2(t) \end{bmatrix} \tag{2}$$

$$\vec{OK} = \begin{bmatrix} -d \cos(\pi/6) \\ +d \sin(\pi/6) \\ s_3(t) \end{bmatrix} \tag{3}$$

vectors  $\vec{IJ}$ ,  $\vec{JK}$  and  $\vec{KI}$  can be written as

$$\begin{cases} \vec{IJ} = \vec{OJ} - \vec{OI} \\ \vec{JK} = \vec{OK} - \vec{OJ} \\ \vec{KI} = \vec{OI} - \vec{OK} \end{cases} \tag{4}$$

Consider Figure 3 which shows points  $I$ ,  $J$ ,  $K$  and  $G$  in the rigid star plane, the  $xy$  plane. Given the vectors  $\vec{IJ}$ ,  $\vec{JK}$  and  $\vec{KI}$ , the locus of the point  $G$  on the rigid star plane such that angles  $\angle IGJ$ ,  $\angle JGK$  and  $\angle KGI$  each equals 120 degrees are on three arcs of three circles on the rigid star plane. The cross section for any two of these arcs identifies the working point of the robot, point  $G$ . For example, by specifying positions of the points  $I$  and  $J$  and the amount of angle  $\angle IGJ = 120^\circ$ , the position of point  $G$  will fall on the circular arc  $IGJ$ . Also, by specifying positions of points  $J$  and  $K$  and the amount of angle  $\angle JGK = 120^\circ$ , the position of point  $G$

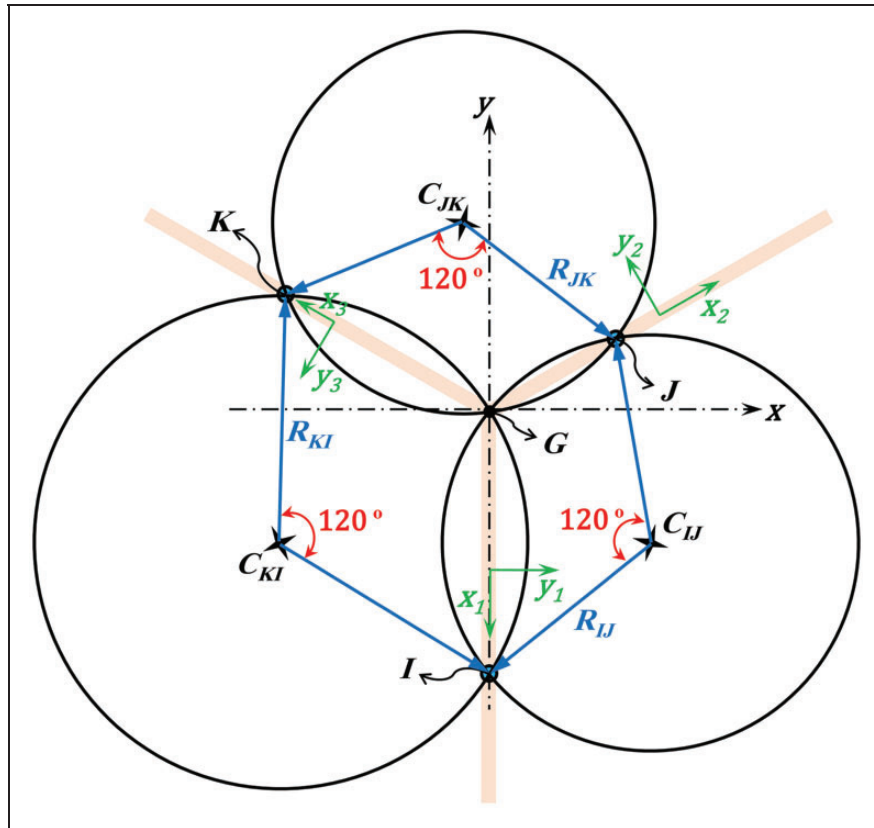


Figure 3. Circles on the rigid star plane which are used to obtain point G.

will fall on the circular arc  $\overset{\frown}{JGK}$ . Therefore, the intersection of the arcs  $\overset{\frown}{IGJ}$  and  $\overset{\frown}{JGK}$  provides position of point  $G$ . Then angle  $\angle KGI$  also equals to  $120^\circ$ .

For the direct kinematics, first, radiuses of the mentioned arcs are obtained using the geometry of the central angle, inscribed angle and triangle. For example, in Figure 3, consider the circle with center point  $C_{IJ}$ . Since the inscribed angle  $\angle IGJ$  equals  $120^\circ$ , the central angle  $\angle IC_{IJ}J$  in triangle  $\Delta IC_{IJ}J$  also equals  $120^\circ$ . Then for the isosceles triangle  $\Delta IC_{IJ}J$ , we have  $|\overrightarrow{IC}_{IJ}| = (|\overrightarrow{IJ}|/2)/\sin(120^\circ/2) = |\overrightarrow{IJ}|/\sqrt{3}$ , or  $R_{IJ} = |\overrightarrow{IJ}|/\sqrt{3}$ . This calculation can also be performed for the circle with center points  $C_{JK}$  and  $C_{KI}$ . Therefore we have

$$R_{IJ} = |\overrightarrow{IJ}|/\sqrt{3}, \quad R_{JK} = |\overrightarrow{JK}|/\sqrt{3}, \quad R_{KI} = |\overrightarrow{KI}|/\sqrt{3} \tag{5}$$

Using the cross product of vector  $\overrightarrow{IJ}$  by vector  $\overrightarrow{JK}$ , the normal unit vector of the rigid star plane is obtained in the fixed coordinate system  $XYZ$  as

$$\hat{N}_{star} = \frac{\overrightarrow{IJ} \otimes \overrightarrow{JK}}{|\overrightarrow{IJ} \otimes \overrightarrow{JK}|} \tag{6}$$

Note that in this paper cross and dot products are shown with  $\otimes$  and  $\odot$ , respectively. Position vectors for the arc centers containing the vectors  $\overrightarrow{IJ}$ ,  $\overrightarrow{JK}$  and  $\overrightarrow{KI}$  can be written as

$$\begin{aligned} \overrightarrow{OC}_{IJ} &= 0.5(\overrightarrow{OI} + \overrightarrow{OJ}) + 0.5 \tan(\pi/6) \overrightarrow{IJ} \otimes \hat{N}_{star} \\ \overrightarrow{OC}_{JK} &= 0.5(\overrightarrow{OJ} + \overrightarrow{OK}) + 0.5 \tan(\pi/6) \overrightarrow{JK} \otimes \hat{N}_{star} \\ \overrightarrow{OC}_{KI} &= 0.5(\overrightarrow{OK} + \overrightarrow{OI}) + 0.5 \tan(\pi/6) \overrightarrow{KI} \otimes \hat{N}_{star} \end{aligned} \tag{7}$$

The position of point  $G$  is located on the intersection of three circular arcs which also lay on the rigid star plane. Consider three spheres with origins at  $C_{IJ}$ ,  $C_{JK}$  and  $C_{KI}$  and radiuses  $R_{IJ}$ ,  $R_{JK}$  and  $R_{KI}$ , respectively. Then, the intersection of the spheres and the rigid star plane identify three circles which also contain the circular arcs  $\overset{\frown}{IGJ}$ ,  $\overset{\frown}{JGK}$  and  $\overset{\frown}{KGI}$ , respectively. Therefore, we can write:

$$\begin{aligned} |\overrightarrow{OG} - \overrightarrow{OC}_{IJ}| &= R_{IJ} \\ |\overrightarrow{OG} - \overrightarrow{OC}_{JK}| &= R_{JK} \end{aligned}$$

$$\begin{aligned} |\overrightarrow{OG} - \overrightarrow{OC}_{KI}| &= R_{KI} \\ (\overrightarrow{OG} - \overrightarrow{OI}) \odot \hat{N}_{star} &= 0 \end{aligned} \tag{8}$$

The last row in equation (8) identifies the rigid star plane. By solving equation (8), which only has one answer, the position vector  $\overrightarrow{OG}$  is obtained. Then, by taking a time derivative, acceleration of point  $G$  in the  $XYZ$  coordinate system,  $\mathbf{a}_G$ , is obtained as

$$\mathbf{a}_G = \frac{d^2}{dt^2} (\overrightarrow{OG}) \tag{9}$$

Now using a common rotation theory for three-dimensional rigid bodies presented by Greenwood (2003), angular velocity of the rigid motion of the star is obtained. First, overall rotation matrix,  $C$ , can be written as

$$C = \begin{bmatrix} \mathbf{i} \odot \mathbf{I} & \mathbf{i} \odot \mathbf{J} & \mathbf{i} \odot \mathbf{K} \\ \mathbf{j} \odot \mathbf{I} & \mathbf{j} \odot \mathbf{J} & \mathbf{j} \odot \mathbf{K} \\ \mathbf{k} \odot \mathbf{I} & \mathbf{k} \odot \mathbf{J} & \mathbf{k} \odot \mathbf{K} \end{bmatrix} \tag{10}$$

in which  $(\mathbf{i}, \mathbf{j}, \mathbf{k})$  are unit vectors of the rigid body coordinate system  $xyz$  and  $(\mathbf{I}, \mathbf{J}, \mathbf{K})$  are unit vectors of the fixed coordinate system  $XYZ$ . According to the definition of the  $xyz$  coordinate system for the 3-PSP robot, the  $y$ -axis is in the opposite direction of vector  $\overrightarrow{GI}$  and the  $z$ -axis is in the same direction as the normal vector of the rigid star plane. Note that  $\overrightarrow{GI} = \overrightarrow{OI} - \overrightarrow{OG}$  and the vectors  $\overrightarrow{OI}$  and  $\overrightarrow{OG}$  are obtained from equations (1) and (8), respectively. Therefore, according to the definition of the  $xyz$  coordinate system, the overall rotation matrix  $C$  can be written as

$$C = \begin{bmatrix} \left( \hat{N}_{star} \otimes \frac{\overrightarrow{GI}}{|\overrightarrow{GI}|} \right)^T \\ - \left( \frac{\overrightarrow{GI}}{|\overrightarrow{GI}|} \right)^T \\ (\hat{N}_{star})^T \end{bmatrix} \tag{11}$$

in which the superscript  $T$  denotes transpose of a matrix or vector. An asymmetric matrix,  $\tilde{\omega}$ , containing components of the angular velocity vector,  $\omega$ , is defined as

$$\tilde{\omega} = \begin{bmatrix} 0 & -\omega_z & \omega_y \\ \omega_z & 0 & -\omega_x \\ -\omega_y & \omega_x & 0 \end{bmatrix}, \quad \omega = \omega_x \mathbf{i} + \omega_y \mathbf{j} + \omega_z \mathbf{k} \tag{12}$$

The matrix  $\tilde{\omega}$  is obtained from the Poisson equation as follows (Greenwood, 2003):

$$\dot{C} = -\tilde{\omega}C \Rightarrow \tilde{\omega} = CC^T \tag{13}$$

Therefore, using equations (12) and (13) the angular velocity vector of the rigid star,  $\omega$ , is obtained. By taking the first derivative of angular velocity  $\omega$ , angular acceleration  $\dot{\omega}$  can be obtained. As shown in Figure 2,  $x_{p1}$ ,  $x_{p2}$  and  $x_{p3}$  represent positions of the three passive prismatic joints in the rigid body coordinate systems,  $x_1y_1z_1$ ,  $x_2y_2z_2$  and  $x_3y_3z_3$ , respectively. Because the vibration amplitude and the slope angle of deformation are small, the distance between point  $G$  and  $G'$  is very small compared with the length of the vectors  $\overrightarrow{GI}$ ,  $\overrightarrow{GJ}$  and  $\overrightarrow{GK}$ . Therefore, the length of the vectors  $\overrightarrow{G'I}$ ,  $\overrightarrow{G'J}$  and  $\overrightarrow{G'K}$  are assumed to be equal to the length of the vectors  $\overrightarrow{GI}$ ,  $\overrightarrow{GJ}$  and  $\overrightarrow{GK}$ , respectively. Consequently:

$$\begin{aligned} x_{p1} &= \left| \overrightarrow{G'I} \right| - L/2, & x_{p2} &= \left| \overrightarrow{G'J} \right| - L/2, \\ x_{p3} &= \left| \overrightarrow{G'K} \right| - L/2 \end{aligned} \tag{14}$$

Upon obtaining rigid acceleration of the point  $G$ , equation (9), the rigid acceleration of each point or element of the moving platform can be obtained. As shown in equation (10), the overall rotation matrix  $C$  can be used as a rotation matrix from  $XYZ$  coordinate system to  $xyz$  coordinate system. Additionally, rotation matrixes from  $xyz$  coordinate system to the  $x_1y_1z_1$ ,  $x_2y_2z_2$  and  $x_3y_3z_3$  coordinate systems are shown with  $R_1$ ,  $R_2$  and  $R_3$ , respectively. Due to the definition of the mentioned rigid body coordinate systems, the above rotation matrixes can be written as follows:

$$\begin{aligned} R_1 &= \begin{bmatrix} 0 & -1 & 0 \\ 1 & 0 & 0 \\ 0 & 0 & 1 \end{bmatrix}, \\ R_2 &= \begin{bmatrix} \cos(\pi/6) & \sin(\pi/6) & 0 \\ -\sin(\pi/6) & \cos(\pi/6) & 0 \\ 0 & 0 & 1 \end{bmatrix}, \\ R_3 &= \begin{bmatrix} -\cos(\pi/6) & \sin(\pi/6) & 0 \\ -\sin(\pi/6) & -\cos(\pi/6) & 0 \\ 0 & 0 & 1 \end{bmatrix} \end{aligned} \tag{15}$$

Consider Figure 2 and an element on the beams 1, 2 or 3. Assume that coordinates of this element in the related coordinate system  $x_iy_iz_i$  is  $[x_i \ 0 \ 0]^T$ . Therefore the distance of the element from point  $G$  is  $(x_i + L/2)$ . Multiplying inverse of the rotation matrixes  $R_1$ ,  $R_2$  and  $R_3$  by  $[(x_i + L/2) \ 0 \ 0]^T$  the position of

the element in the  $xyz$  coordinate system is obtained as follows:

$$\begin{aligned} \mathbf{r}_1 &= \begin{bmatrix} 0 \\ -(x_i + L/2) \\ 0 \end{bmatrix}, \\ \mathbf{r}_2 &= \begin{bmatrix} (x_i + L/2) \cos(\pi/6) \\ (x_i + L/2) \sin(\pi/6) \\ 0 \end{bmatrix}, \\ \mathbf{r}_3 &= \begin{bmatrix} -(x_i + L/2) \cos(\pi/6) \\ (x_i + L/2) \sin(\pi/6) \\ 0 \end{bmatrix} \end{aligned} \quad (16)$$

Rigid acceleration components of the element in the  $x_i$ ,  $y_i$  and  $z_i$  directions are  $a_{xi}(x_i, t)$ ,  $a_{yi}(x_i, t)$  and  $a_{zi}(x_i, t)$ , respectively. Therefore, for the element in the rigid body coordinate  $x_i y_i z_i$ , it can be written:

$$\begin{bmatrix} a_{xi}(x_i, t) \\ a_{yi}(x_i, t) \\ a_{zi}(x_i, t) \end{bmatrix} = \mathbf{R}_i [\mathbf{C} \mathbf{a}_G + \boldsymbol{\omega} \otimes (\boldsymbol{\omega} \otimes \mathbf{r}_i) + \dot{\boldsymbol{\omega}} \otimes \mathbf{r}_i], \quad i = 1, 2, 3 \quad (17)$$

Note that the rigid acceleration components of the element  $a_{xi}(x_i, t)$ ,  $a_{yi}(x_i, t)$  and  $a_{zi}(x_i, t)$  depend on the position of the element and time trajectory of the three inputs of the robot. The component  $a_{xi}(x_i, t)$  is in the axial direction of the beam number  $i$  and the components  $a_{yi}(x_i, t)$  and  $a_{zi}(x_i, t)$  are in its transverse directions. These accelerations are used in motion equations of the beams. To consider the effect of the gravity in the motion equations, we must add gravitational acceleration to rigid acceleration of the star. Therefore, for the motion equations, we use  $(\mathbf{a}_G - \mathbf{g})$  instead of  $\mathbf{a}_G$  in equation (17) in which  $\mathbf{g} = [0 \ 0 \ -9.81]^T (m/s^2)$ .

#### 4. Constraint equations for center point of the moving star

In Figure 4, unit vector  $\hat{N}'_{star}$  represents the normal vector on the deformed moving star at point  $G'$  in the rigid body coordinate system  $xyz$ . Next, consider unit vectors  $\hat{u}_i$ ,  $\hat{v}_i$  and  $\hat{w}_i$  of the rigid body coordinate system  $x_i y_i z_i$ . Each of these unit vectors ( $\hat{u}_i$ ,  $\hat{v}_i$ ,  $\hat{w}_i$ ) are defined in the  $xyz$  rigid body coordinate system. Note that  $\hat{w}_i$  is equal to the unit vector  $\mathbf{k}$ . Parameter  $\theta_{Gi}$  represents the angle between the axis  $x_i$  and the neutral axis of the beam  $i$  at point  $G'$ . The following equation can be written:

$$\tan(\theta_{Gi}) = \left. \frac{\partial w_i}{\partial x_i} \right|_{x_i = -L/2}, \quad i = 1, 2, 3 \quad (18)$$

As assumed in Section 2, elastic displacement of the moving star is only in  $w_i$ -direction and therefore the neutral axis of the beam  $i$  is located in  $x_i z_i$  plane. We can decompose the unit vector  $\hat{N}'_{star}$  to two components. First, its image on the plane  $x_i z_i$  which is called  $\vec{N}'_{star}{}^{x_i z_i}$  and second, its normal component to the plane  $x_i z_i$  which is in  $y_i$ -direction and is called  $\vec{N}'_{star}{}^{y_i}$ . Note that the component  $\vec{N}'_{star}{}^{x_i z_i}$  is normal to the neutral axis of the beam  $i$  at point  $G'$  then using the component  $\vec{N}'_{star}{}^{x_i z_i}$  we can write

$$\begin{aligned} \vec{N}'_{star}{}^{x_i z_i} \odot \hat{u}_i &= \left| \vec{N}'_{star}{}^{x_i z_i} \right| \cos(\theta_{Gi} + \pi/2) \\ &= - \left| \vec{N}'_{star}{}^{x_i z_i} \right| \sin(\theta_{Gi}), \quad i = 1, 2, 3 \end{aligned} \quad (19)$$

$$\vec{N}'_{star}{}^{x_i z_i} \odot \hat{w}_i = \left| \vec{N}'_{star}{}^{x_i z_i} \right| \cos(\theta_{Gi}), \quad i = 1, 2, 3 \quad (20)$$

Dividing equation (19) by equation (20), gives

$$\frac{\vec{N}'_{star}{}^{x_i z_i} \odot \hat{u}_i}{\vec{N}'_{star}{}^{x_i z_i} \odot \hat{w}_i} = -\tan(\theta_{Gi}), \quad i = 1, 2, 3 \quad (21)$$

Because the component  $\vec{N}'_{star}{}^{y_i}$  is normal to the vectors  $\hat{u}_i$  and  $\hat{w}_i$  then

$$\vec{N}'_{star}{}^{x_i z_i} \odot \hat{u}_i = \left( \vec{N}'_{star}{}^{x_i z_i} + \vec{N}'_{star}{}^{y_i} \right) \odot \hat{u}_i = \hat{N}'_{star} \odot \hat{u}_i, \quad i = 1, 2, 3 \quad (22)$$

$$\vec{N}'_{star}{}^{x_i z_i} \odot \hat{w}_i = \left( \vec{N}'_{star}{}^{x_i z_i} + \vec{N}'_{star}{}^{y_i} \right) \odot \hat{w}_i = \hat{N}'_{star} \odot \hat{w}_i, \quad i = 1, 2, 3 \quad (23)$$

Substituting equations (22) and (23) into equation (21) and using  $\hat{w}_i = \mathbf{k}$  gives

$$\frac{\hat{N}'_{star} \odot \hat{u}_i}{\hat{N}'_{star} \odot \mathbf{k}} = -\tan(\theta_{Gi}), \quad i = 1, 2, 3 \quad (24)$$

Note that the three unit vectors  $\hat{u}_1$ ,  $\hat{u}_2$  and  $\hat{u}_3$  are each along axis  $x_1$ ,  $x_2$  and  $x_3$  respectively. These unit vectors are all in the rigid star plane and make an angle of  $120^\circ$  with each other. Therefore, we have  $(\hat{u}_1 + \hat{u}_2 + \hat{u}_3) = 0$ . Summing three equations of (24), we have

$$\begin{aligned} &\tan(\theta_{G1}) + \tan(\theta_{G2}) + \tan(\theta_{G3}) \\ &= - \left( \frac{\hat{N}'_{star}}{\hat{N}'_{star} \odot \mathbf{k}} \right) \odot (\hat{u}_1 + \hat{u}_2 + \hat{u}_3) = 0 \end{aligned} \quad (25)$$

Finally, using equation (18) and equation (25), an important constraint between the slopes of the

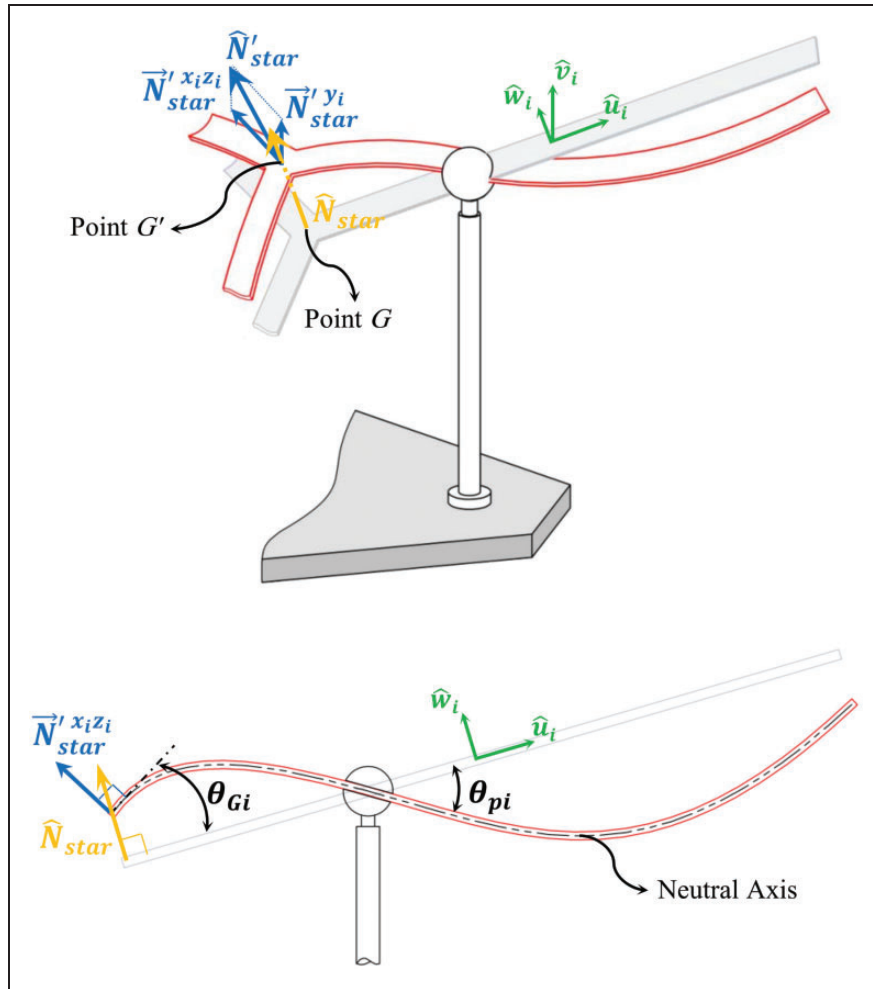


Figure 4. Magnified view of the elastic displacement of point G.

three beams at their junction point  $G'$  is obtained as

$$\frac{\partial w_1}{\partial x_1} \Big|_{x_1=-L/2} + \frac{\partial w_2}{\partial x_2} \Big|_{x_2=-L/2} + \frac{\partial w_3}{\partial x_3} \Big|_{x_3=-L/2} = 0 \quad (26)$$

Additionally, because all three beams are connected at point  $G'$ , two additional constraints can be written between the elastic displacements of the three beams as

$$w_1 \left( -\frac{L}{2}, t \right) = w_2 \left( -\frac{L}{2}, t \right) = w_3 \left( -\frac{L}{2}, t \right) \quad (27)$$

### 5. Motion equation and applying the constraints

The dynamics of parallel robots can be viewed as both direct and inverse problems. In the direct

dynamics, motor torques/forces are supplied and the resulting robot motion is obtained. Conversely, in the inverse dynamic problem, the motion of the robot is supplied and required motor torques/forces are obtained. In this section, a dynamics model of the 3-PSP parallel robot is developed which can be used for both the direct and inverse dynamic problem.

Sharifnia and Akbarzadeh (2014a), have presented a motion equation for planar vibrational motion of a Euler-Bernoulli beam with a prismatic joint in virtual form. Similar to the present study, the authors assumed both the vibration amplitude and the slope angle of elastic displacements to be small in their analytical model. In the present research, the same motion equation is developed and relevant constraint equations are applied to the motion equation using Lagrange's multipliers. For an element of the flexible star at  $x_i$  position, the motion equation in the

$z_i$ -direction can be written as

$$\begin{aligned} & \left[ \rho \left( \frac{\partial^2 w_i}{\partial t^2} - w_i(\omega_x^2 + \omega_y^2) \right) + \frac{\partial^2}{\partial x_i^2} \left( EI \frac{\partial^2 w_i}{\partial x_i^2} \right) \right. \\ & \left. + \frac{\partial}{\partial x_i} \left( \rho(L - x_i) a_{xi} \left( \frac{x_i + L}{2}, t \right) \frac{\partial w_i}{\partial x_i} \right) \right] \delta w_i(x_i) \\ & = -\rho a_{zi}(x_i, t) \delta w_i(x_i) + F_{pi} \text{dirac}(x_i - x_{pi}) \delta w_i(x_{pi}) \\ & \quad i = 1, 2, 3 \end{aligned} \tag{28}$$

in which parameters  $L$ ,  $EI$  and  $\rho$  represent the beam length, bending rigidity and mass per length, respectively, and have the same values for all the three beams of the star. Note that the magnitude of the vector  $\omega$  is the same in the  $x_i y_i z_i$  and  $xyz$  rigid body coordinate systems. Additionally, their  $z_i$ -axis are in the same direction. Therefore, we have  $(\omega_x^2 + \omega_y^2) = (\omega_{xi}^2 + \omega_{yi}^2)$ . The expression  $\partial^2 w_i / \partial t^2$  is the relative acceleration of the element in the  $x_i y_i z_i$  rigid body coordinate system in the  $z_i$ -direction. Similarly, the expression  $-w_i(\omega_x^2 + \omega_y^2)$  is the relative acceleration of the element due to its elastic motion and rigid rotational motion in the  $x_i y_i z_i$  rigid body coordinate system in the  $z_i$ -direction. Therefore, the expression  $\rho(\partial^2 w_i / \partial t^2 - w_i(\omega_x^2 + \omega_y^2))$  is the inertia force due to the elastic motion of the element. The expression  $\partial^2(EI \partial^2 w_i / \partial x_i^2) / \partial x_i^2$  represents the result of shear forces at two sides of the element. The term of  $\partial[\rho(L - x_i) a_{xi}(x_i, t) (\partial w_i / \partial x_i)] / \partial x_i$  represents the result of axial inertia forces on two sides of the element in the  $z_i$ -direction. The expression  $\rho a_{zi}(x_i, t)$  represents the inertia force due to the rigid motion of the element in the  $z_i$ -direction. The parameter  $F_{pi}$  is the result of normal contact forces applied to the beam  $i$  at  $x_i = x_{pi}$  by the prismatic joint in the  $z_i$ -direction. For virtual deflection of  $\delta w_i(x_i)$ , the sum of the virtual works of the mentioned inertia forces and the shear force must be equal to the virtual work of the force  $F_{pi}$ . Using this equilibrium condition, the motion equation (28) is obtained for the beam element. For more details please see Sharifnia and Akbarzadeh (2014a). Additionally, parameters  $x_{pi}$ ,  $a_{zi}(x_i, t)$  and  $a_{xi}((x_i + L)/2, t)$  are determined by equations (14) and (17). All friction forces are assumed to be negligible.

The term of  $\partial[\rho(L - x_i) a_{xi}(x_i, t) (\partial w_i / \partial x_i)] / \partial x_i$  used in motion equation (28) can be expanded as follows:

$$\begin{aligned} & \frac{\partial}{\partial x_i} \left( \rho(L - x_i) a_{xi} \left( \frac{x_i + L}{2}, t \right) \frac{\partial w_i}{\partial x_i} \right) \\ & = -\rho a_{xi} \left( \frac{x_i + L}{2}, t \right) \frac{\partial w_i}{\partial x_i} + \rho(L - x_i) \frac{\partial a_{xi} \left( \frac{x_i + L}{2}, t \right)}{\partial x_i} \frac{\partial w_i}{\partial x_i} \\ & \quad + \rho(L - x_i) a_{xi} \left( \frac{x_i + L}{2}, t \right) \frac{\partial^2 w_i}{\partial x_i^2} \approx 0 \end{aligned} \tag{29}$$

The values of the above expression are negligible due to the assumption of a small slope angle for the elastic displacement of the beams (Sharifnia and Akbarzadeh, 2014a). Consequently, compared with the other terms of equation (28), the expression mentioned in equation (29) may be neglected.

To apply the constraint equations (26) and (27) into the motion equation, they are written in the form of virtual displacement as

$$\begin{aligned} & M_G \left( \delta \left( \frac{\partial w_1}{\partial x_1} \Big|_{x_1=-L/2} \right) + \delta \left( \frac{\partial w_2}{\partial x_2} \Big|_{x_2=-L/2} \right) \right. \\ & \left. + \delta \left( \frac{\partial w_3}{\partial x_3} \Big|_{x_3=-L/2} \right) \right) = 0 \end{aligned} \tag{30}$$

$$\begin{cases} V_{G1} \left( \delta w_1 \left( -\frac{L}{2} \right) - \delta w_2 \left( -\frac{L}{2} \right) \right) = 0 \\ V_{G3} \left( \delta w_3 \left( -\frac{L}{2} \right) - \delta w_2 \left( -\frac{L}{2} \right) \right) = 0 \end{cases} \tag{31}$$

in which the parameter  $M_G$  is the proper Lagrange's multiplier that represents a bending moment for all the three beams at point  $G'$ . The parameters  $V_{G1}$  and  $V_{G3}$  are proper Lagrange's multipliers that represent shear forces for beams 1 and 3 at the point  $G'$ , respectively. As can be seen from equation (31), virtual work of  $V_{G1}$  and  $V_{G3}$  are  $V_{G1} \delta w_1(-L/2)$  and  $V_{G3} \delta w_3(-L/2)$  due to the virtual displacements of  $\delta w_1(-L/2)$  and  $\delta w_3(-L/2)$ , respectively. In addition, their virtual work is  $(-V_{G1} - V_{G3}) \delta w_2(-L/2)$  in which the coefficient of virtual displacement of  $\delta w_2(-L/2)$  represents the value of  $V_{G2}$ . Therefore  $V_{G2} = -V_{G1} - V_{G3}$ . This shows the equilibrium of shear forces at the point  $G'$ ,

$$V_{G1} + V_{G2} + V_{G3} = 0 \tag{32}$$

By means of equation (32) an external load in the  $z$ -direction can be applied in the presented model. If an external vertical force,  $V_{ext}$ , is applied in point  $G$ , then instead of equation (32) there is

$$V_{G1} + V_{G2} + V_{G3} = V_{ext} \tag{32a}$$

Additional constraints are written for displacement of points on the star where the prismatic joints are located, as follows:

$$F_{pi} \delta w_i(x_{pi}) = 0 \quad i = 1, 2, 3 \tag{33}$$

Note that the constraint equation (33) is already applied in the motion equation (28). As mentioned earlier, the Lagrange multiplier  $F_{pi}$  is resultant of normal contact forces that the prismatic joint applies to the

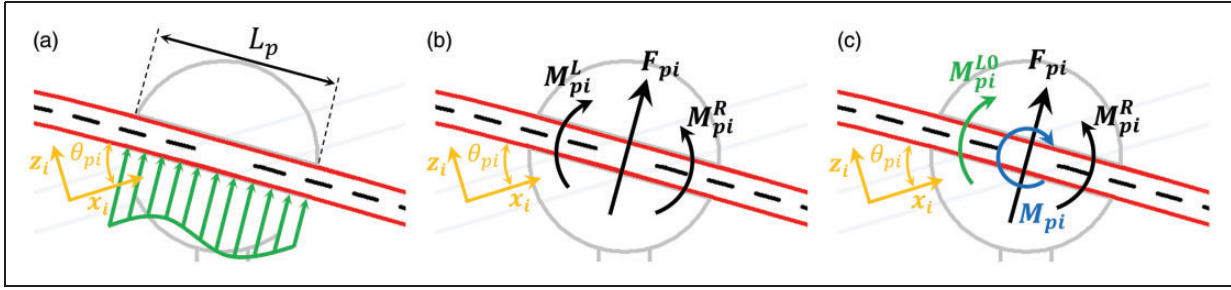


Figure 5. Dynamic model of the passive prismatic joint.

beam at  $x_i = x_{pi}$ . The effect of the physical length of the passive prismatic joints on the vibrational behavior of the flexible links was previously studied by Sharifnia and Akbarzadeh (2014a,b). When the ratio of exciting load per stiffness of the links is high, a longer length of the passive prismatic joint significantly increases the stiffness of the flexible link. In the present paper, the bending stiffness of the flexible beams of the star is relatively high, so that the physical length of the prismatic joints does not influence the vibrational behavior of the beams.

Consider Figure 5. Normal contact forces that the prismatic joint  $i$  applies to the beam  $i$  can be modeled as a distributed force on the beam (Figure 5(a)). This distributed force can be simplified by the resultant contact force  $F_{pi}$  (equation (33)) and two moments,  $M_{pi}^L$  and  $M_{pi}^R$ , (Figure 5(b)). Next  $M_{pi}^L$  is decomposed into resultant of the two moments  $M_{pi} = M_{pi}^L - M_{pi}^R$  and  $M_{pi}^{L0} = M_{pi}^R$  (Figure 5(c)). Therefore, virtual work of the two equal moments  $M_{pi}^{L0}$  and  $M_{pi}^R$  applied by the rigid passive prismatic joint can be written as

$$\begin{aligned}
 & M_{pi}^R \delta \left( \frac{\partial w_i}{\partial x_i} \Big|_{x_i=x_{pi}^R} \right) - M_{pi}^{L0} \delta \left( \frac{\partial w_i}{\partial x_i} \Big|_{x_i=x_{pi}^L} \right) \\
 &= M_{pi}^{L0} \delta \left( \frac{\partial w_i}{\partial x_i} \Big|_{x_i=x_{pi}^R} - \frac{\partial w_i}{\partial x_i} \Big|_{x_i=x_{pi}^L} \right) \\
 &= M_{pi}^{L0} (x_{pi}^R - x_{pi}^L) \delta \left( \frac{\partial^2 w_i}{\partial x_i^2} \Big|_{x_i=x_{pi}} \right) \\
 &= N_{pi} \delta \left( \frac{\partial^2 w_i}{\partial x_i^2} \Big|_{x_i=x_{pi}} \right) \equiv 0 \\
 &\Rightarrow N_{pi} \delta \left( \frac{\partial^2 w_i}{\partial x_i^2} \Big|_{x_i=x_{pi}} \right) = 0 \tag{34}
 \end{aligned}$$

in which  $x_{pi}^R$  and  $x_{pi}^L$  are two unspecified locations for the two moments  $M_{pi}^{L0}$  and  $M_{pi}^R$ . Equation (34) imposes a constraint of zero curvature at the location of the passive prismatic joints and is applied in the dynamic model for each passive prismatic joint. The Lagrange's multiplier  $N_{pi} = M_{pi}^{L0} (x_{pi}^R - x_{pi}^L)$  causes curvature of the

beam  $i$  at point  $x_i = x_{pi}$  to vanish. Figure 6 shows a free body diagram for the moving star and one of the three legs of the robot. Note that couples and forces are shown by the double-arrow and single-arrow vectors, respectively.

Next, the effect of rotational moment of inertia for the passive prismatic joints on the beam in the dynamic model can be considered. The angle of the passive prismatic joint with respect to  $x_i$ -axis is called  $\theta_{pi}$ . Therefore, an additional constraint at point  $x_i = x_{pi}$  can be written as

$$\begin{aligned}
 \theta_{pi} &= \frac{\partial w_i(x_i, t)}{\partial x_i} \Big|_{x_i=x_{pi}} = \frac{\partial w_i}{\partial x_i}(x_{pi}, t) \\
 \Rightarrow M_{pi} \left( \delta \theta_{pi} - \delta \frac{\partial w_i}{\partial x_i}(x_{pi}) \right) &= 0 \quad i = 1, 2, 3 \tag{35}
 \end{aligned}$$

in which  $M_{pi}$  is a Lagrange's multiplier and represents the resultant moment that the rigid prismatic joint applies on the corresponding beam. According to constraint equation (35), the angular positions of the passive prismatic joints,  $\theta_{pi}$ , are included in the dynamic model. Then, to solve for  $\theta_{pi}$ , motion differential equations for angular motion of the passive prismatic joints are obtained by considering Euler equations, the virtual work principle and equation (35) as follows:

$$\begin{aligned}
 & \left( I_{yy}^p \left( \frac{d^2 \theta_{pi}}{dt^2} + \dot{\omega}_{yi} \right) + (I_{xx}^p - I_{zz}^p) \omega_{zi} \omega_{xi} \right) \delta \theta_{pi} = M_{pi} \delta \theta_{pi} \\
 & \Delta I_{yy}^p \left( \frac{d^2 \theta_{pi}}{dt^2} + \dot{\omega}_{yi} \right) + (I_{xx}^p - I_{zz}^p) \omega_{zi} \omega_{xi} = M_{pi} \\
 & i = 1, 2, 3 \tag{36}
 \end{aligned}$$

in which  $I_{xx}^p$ ,  $I_{yy}^p$  and  $I_{zz}^p$  are principal moments of inertia for each passive prismatic joint in the  $x_i y_i z_i$  coordinate system and  $\dot{\omega}_{yi}$  is the  $y_i$ -component of angular acceleration of the rigid star. The above differential equation (36) is a motion equation for the rotational motion of the passive prismatic joints and must be simultaneously solved with the other motion and constraint equations. Neglecting the small terms of the equation (29) and

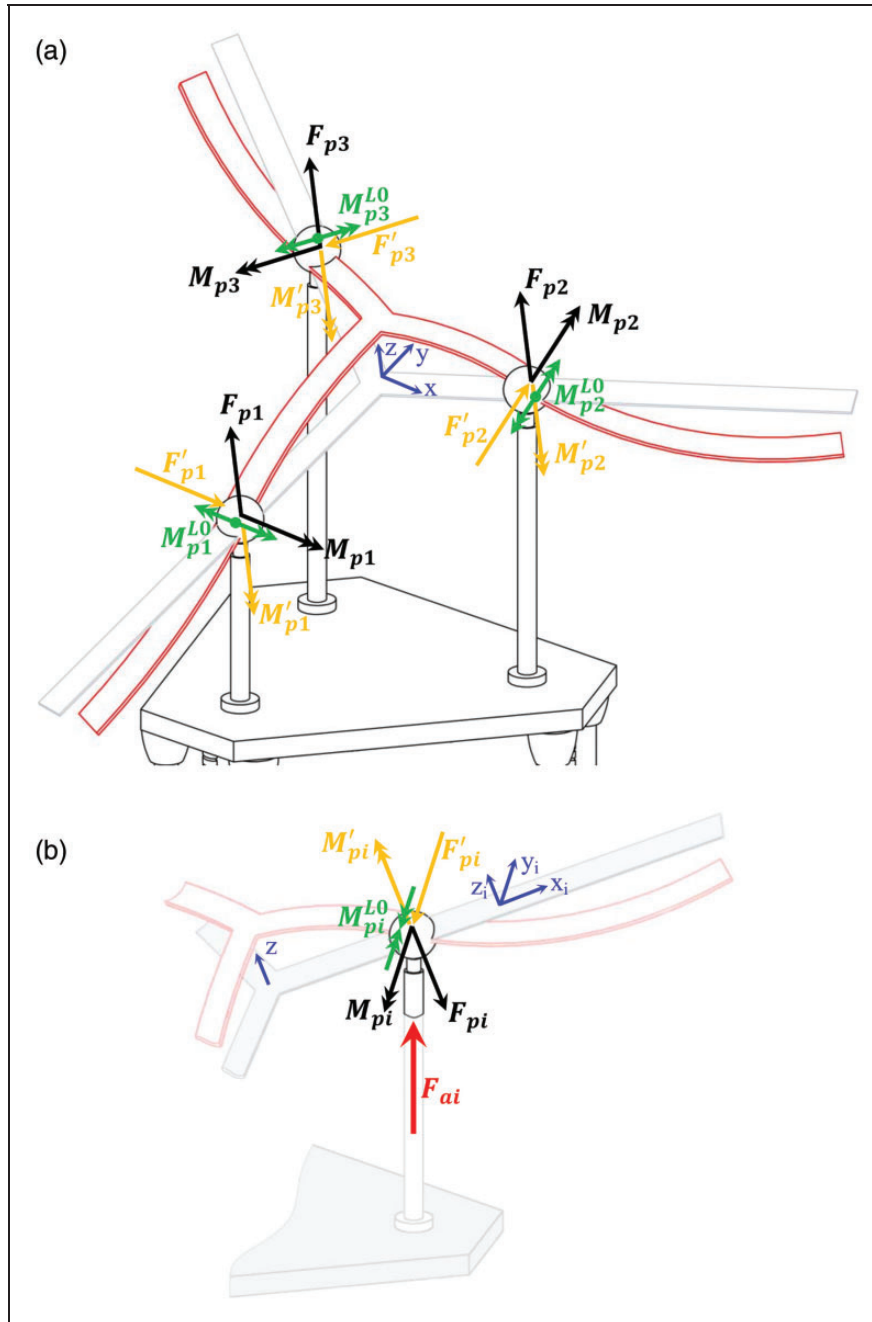


**Figure 6.** (a) Free body diagram of the moving star; (b) free body diagram for one of the three legs.

applying the constraint equations (30) up to (35) with relevant Lagrange's multipliers, the motion equation for each beam of the moving platform, equation (28), can be obtained as

$$\left[ \rho \left( \frac{\partial^2 w_i}{\partial t^2} - w_i (\omega_x^2 + \omega_y^2) \right) + \frac{\partial^2}{\partial x_i^2} \left( EI \frac{\partial^2 w_i}{\partial x_i^2} \right) \right] \delta w_i(x_i) = -\rho a_{zi}(x_i, t) \delta w_i(x_i) + F_{pi} \text{dirac}(x_i - x_{pi}) \delta w_i(x_{pi})$$

$$\begin{aligned} & - M_{pi} \text{dirac}(x_i - x_{pi}) \delta \frac{\partial w_i}{\partial x_i}(x_{pi}) \\ & + N_{pi} \text{dirac}(x_i - x_{pi}) \delta \frac{\partial^2 w_i}{\partial x_i^2}(x_{pi}) \\ & + V_{Gi} \text{dirac} \left( x_i + \frac{L}{2} \right) \delta w_i \left( -\frac{L}{2} \right) \\ & + M_G \text{dirac} \left( x_i + \frac{L}{2} \right) \delta \frac{\partial w_i}{\partial x_i} \left( -\frac{L}{2} \right) \quad i = 1, 2, 3 \quad (37) \end{aligned}$$

In order to obtain the vibration response of the 3-PSP robot, the motion equations, equation (36) and equation (37), must be simultaneously solved with the constraint equations (30) up to (35). Upon solving these equations, the vibration response and Lagrange’s multipliers i.e. constraint forces are determined.

As seen in equation (37) for the beam  $i$ , the normal force  $F_{pi}$  and the moment  $M_{pi}$  are obtained from the vibrational motion equation. The additional normal force and moment of the passive prismatic joint,  $F'_{pi}$  and  $M'_{pi}$ , can be obtained from rigid body dynamics of the moving star. As assumed before, the moving star has no in-plane vibration, i.e. the star is assumed to be rigid in the rigid star plane. For the rigid star, the axes of the rigid body coordinate system  $xyz$  are also principal axes for the moment of inertia. Assuming a total mass of  $m$  and beams length of  $L$  for the rigid star, gives

$$I_{xx} = \frac{1}{6}mL^2, \quad I_{yy} = \frac{1}{6}mL^2, \quad I_{zz} = \frac{1}{3}mL^2, \quad m = 3\rho L \tag{38}$$

In the rigid star plane (see Figure 6), using the Euler equations the following can be written:

$$\begin{aligned} I_{zz}\dot{\omega}_z + (I_{yy} - I_{xx})\omega_x\omega_y &= M_z \\ \Rightarrow (mL^2/3)\dot{\omega}_z &= F'_{p1}(x_{p1} + L/2) - M'_{p1} \\ &+ F'_{p2}(x_{p2} + L/2) - M'_{p2} + F'_{p3}(x_{p3} + L/2) - M'_{p3} \end{aligned} \tag{39}$$

in which  $M'_{pi} = [I'_{zz}\dot{\omega}_{zi} + (I'_{yy} - I'_{xx})\omega_{xi}(\omega_{yi} + d\theta_{pi}/dt)]$ . Also, using the Newton’s second law in the rigid star plane gives

$$\begin{aligned} (\mathbf{F})_{xy} &= m(\mathbf{a}_G)_{xy} \\ \Rightarrow \begin{cases} F'_{p1} - F'_{p2}\sin(\pi/6) - F'_{p3}\sin(\pi/6) = m(C(\mathbf{a}_G - \mathbf{g})) \odot i \\ +F'_{p2}\cos(\pi/6) - F'_{p3}\cos(\pi/6) = m(C(\mathbf{a}_G - \mathbf{g})) \odot j \end{cases} \end{aligned} \tag{40}$$

Using the three equations, equation (39) and (40), the remaining three forces of the passive prismatic joints are obtained. Additionally, having the mass of the passive prismatic joint,  $m_p$ , the mass of the passive spherical joint,  $m_s$ , and the mass of the rigid link (linear rod) of the robot,  $m_l$ , required driving forces,  $F_{ai}$ , can be determined as follows:

$$\begin{aligned} (m_p + m_s + m_l)(\ddot{s}_i(t) + g) &= F_{ai} - F_{pi}\hat{N}_{star} \\ \odot \mathbf{K} - F'_{pi}(C^{-1}R_i^{-1}[0 \ 1 \ 0]^T) \odot \mathbf{K} & \tag{41} \\ g &= 9.8(\text{m/s}^2) \quad \text{and} \quad i = 1, 2, 3 \end{aligned}$$

Upon obtaining  $F_{ai}$ , the inverse dynamics problem of the 3-PSP robot is completed. It should be noted that the same formulation allows the direct dynamics problem of the robot to be solved. This may be accomplished by specifying the driving forces,  $F_{ai}$ , in equation (41) and solving a new set of motion equations (36), (37) and (41) simultaneously with the constraint equations (30) up to (35).

### 6. Solution of the motion equations

In this section, the “constrained assumed modes method” previously used by Sharifnia and Akbarzadeh (2014a,b) is also used to solve the derived motion equations of the 3-PSP parallel robot. Different motions of the robot can induce different acceleration and inertia forces and consequently different boundary conditions at the junction point of the substructures of the moving platform. Therefore, in order to solve the dynamic equations of the robot, two different types of mode shapes for the three Euler-Bernoulli beams are used for three different motion types. Using a combination of mode shapes of the Euler-Bernoulli beam, transverse vibration of the three beams of the star can be written as

$$w_i(x_i, t) = \sum_{m=1}^N \alpha_{im}(t)\varphi_m(x_i) \quad i = 1, 2, 3 \tag{42}$$

in which  $\varphi_m(x_i)$  represents mode shape function of Euler-Bernoulli beam and is

$$\begin{aligned} \varphi_m(x) &= A_m \sin(\beta_m x) + B_m \cos(\beta_m x) \\ &+ C_m \sinh(\beta_m x) + D_m \cosh(\beta_m x) \\ \Rightarrow \left(\frac{EI}{\rho}\right) \frac{\partial^4 \varphi_m}{\partial x^4} &= \lambda_m \varphi_m, \quad \lambda_m = \omega_m^2 = \frac{EI}{\rho} \beta_m^4 \end{aligned} \tag{43}$$

Then, the variation of transverse vibration is written as

$$\delta w_i(x_i, t) = \sum_{m=1}^N \varphi_m(x_i)\delta\alpha_{im}(t) \quad i = 1, 2, 3 \tag{44}$$

Substituting equations (42), (43) and (44) in the motion equation (37) gives

$$\begin{aligned} &\left[ \sum_{m=1}^N \varphi_m(x_i)\ddot{\alpha}_{im}(t) + \left(\lambda_m - (\omega_x^2 + \omega_y^2)\right) \sum_{m=1}^N \varphi_m(x_i)\alpha_{im}(t) \right] \\ &\times \sum_{j=1}^N \varphi_j(x_i)\delta\alpha_{ij}(t) \end{aligned}$$

$$\begin{aligned}
 &= -a_{zi}(x_i, t) \sum_{j=1}^N \varphi_j(x_i) \delta \alpha_{ij}(t) + \frac{F_{pi}}{\rho} \text{dirac}(x_i - x_{pi}) \\
 &\times \sum_{j=1}^N \varphi_j(x_{pi}) \delta \alpha_{ij}(t) - \frac{M_{pi}}{\rho} \text{dirac}(x_i - x_{pi}) \\
 &\times \sum_{j=1}^N \varphi'_j(x_{pi}) \delta \alpha_{ij}(t) + \frac{N_{pi}}{\rho} \text{dirac}(x_i - x_{pi}) \\
 &\times \sum_{j=1}^N \varphi''_j(x_{pi}) \delta \alpha_{ij}(t) + \frac{V_{Gi}}{\rho} \text{dirac}\left(x_i + \frac{L}{2}\right) \\
 &\times \sum_{j=1}^N \varphi_j\left(-\frac{L}{2}\right) \delta \alpha_{ij}(t) + \frac{M_G}{\rho} \text{dirac}\left(x_i + \frac{L}{2}\right) \\
 &\times \sum_{j=1}^N \varphi'_j\left(-\frac{L}{2}\right) \delta \alpha_{ij}(t) \quad i = 1, 2, 3 \tag{45}
 \end{aligned}$$

Considering orthogonality of mode shapes, the above equations are integrated along the length of the beams. Next, separating the equations due to coefficients  $\delta \alpha_{ij}(t)$ , the following ordinary differential equations are obtained:

$$\begin{aligned}
 &\ddot{\alpha}_{ij}(t) + \left(\lambda_j - (\omega_x^2 + \omega_y^2)\right) \alpha_{ij}(t) \\
 &= - \sum_{m=1}^N \int_0^L (a_{zi}(x_i, t) \varphi_j(x_i) dx_i) + \frac{F_{pi}}{\rho} \varphi_j(x_{pi}) - \frac{M_{pi}}{\rho} \varphi'_j(x_{pi}) \\
 &- \frac{N_{pi}}{\rho} \varphi''_j(x_{pi}) + \frac{V_{Gi}}{\rho} \varphi_j\left(-\frac{L}{2}\right) + \frac{M_G}{\rho} \varphi'_j\left(-\frac{L}{2}\right) \\
 &j = 1, \dots, N \quad \text{and} \quad i = 1, 2, 3 \tag{46}
 \end{aligned}$$

Note that equation (46) includes  $3N$  number of independent motion equations. In addition, using equations (42), (43) and (44), the constraint equations, equation (30) up to (35), can be written as

$$\sum_{j=1}^N \varphi'_j\left(-\frac{L}{2}\right) (\alpha_{1j}(t) + \alpha_{2j}(t) + \alpha_{3j}(t)) = 0 \tag{47}$$

$$\begin{cases} \sum_{j=1}^N \varphi_j\left(-\frac{L}{2}\right) (\alpha_{1j}(t) - \alpha_{2j}(t)) = 0 \\ \sum_{j=1}^N \varphi_j\left(-\frac{L}{2}\right) (\alpha_{3j}(t) - \alpha_{2j}(t)) = 0 \end{cases} \tag{48}$$

$$V_{G1} + V_{G2} + V_{G3} = 0 \tag{49}$$

$$\sum_{j=1}^N \varphi_j(x_{pi}) \alpha_{ij}(t) = 0 \quad i = 1, 2, 3 \tag{50}$$

$$\sum_{j=1}^N \varphi''_j(x_{pi}) \alpha_{ij}(t) = 0 \quad i = 1, 2, 3 \tag{51}$$

$$\theta_{pi} - \sum_{j=1}^N \varphi'_j(x_{pi}) \alpha_{ij}(t) = 0 \quad i = 1, 2, 3 \tag{52}$$

To obtain the unknown parameters  $\alpha_{ij}(t)$  and  $\theta_{pi}(t)$ , the motion equations (36) and (46) must be solved together with the constraint equations (47) up to (52). In addition, the solution provides the constraint forces/moments or the Lagrange's multipliers.

### 7. Numerical results

In this section, three case studies each with a different motion trajectory for the moving star are considered as follows:

Case study 1: Rectilinear translation in the  $Z$ -direction, as

$$s_1(t) = s_2(t) = s_3(t) = 0.5 + t^2$$

Case study 2: Rotation about and translation along the  $y$ -direction, as

$$s_1(t) = 0.5, s_2(t) = 0.5 + t^2, s_3(t) = 0.5 - t^2$$

Case study 3: Rotation about the line  $JK$  and translation normal to the line  $JK$ , as

$$s_1(t) = 0.5, \quad s_2(t) = 0.5 + t^2, \quad s_3(t) = 0.5 + t^2$$

Note that as stated in Section 3, the gravitational acceleration is also considered in the above case studies. As mentioned before, at the start of motion for all three cases, the  $xy$  plane (the rigid star plane) is parallel to the  $XY$  plane and also the  $z$  and  $Z$ -axis are collinear. Therefore, at the start of motion we have  $s_1(0) = s_2(0) = s_3(0) = 0.5$  and  $x_{p1}(0) = x_{p2}(0) = x_{p3}(0) = -L/2 + d$ . For each of the three case studies, two different groups of mode shapes are used to solve the motion equations. To do this, consider the working point of the star, point  $G$ , and assume two different boundary conditions of slide and free. For the free ends of the beams, points  $A$ ,  $B$ , and  $C$ , we use only the free boundary conditions. Therefore, the first group uses slide-free mode shapes, and the second group uses free-free mode shapes. Finally, the results of the approximate analytical solution are compared with the results of a commercial FEM software. For each case study, the numbers of the slide-free and free-free mode shapes used in the approximate analytical solution are 36 and 50, respectively and the number

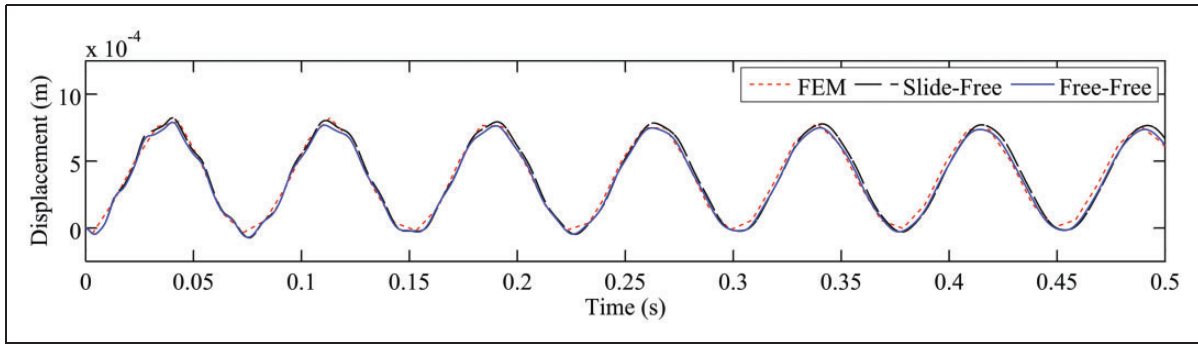


Figure 7. Case study I: elastic displacement of point G.

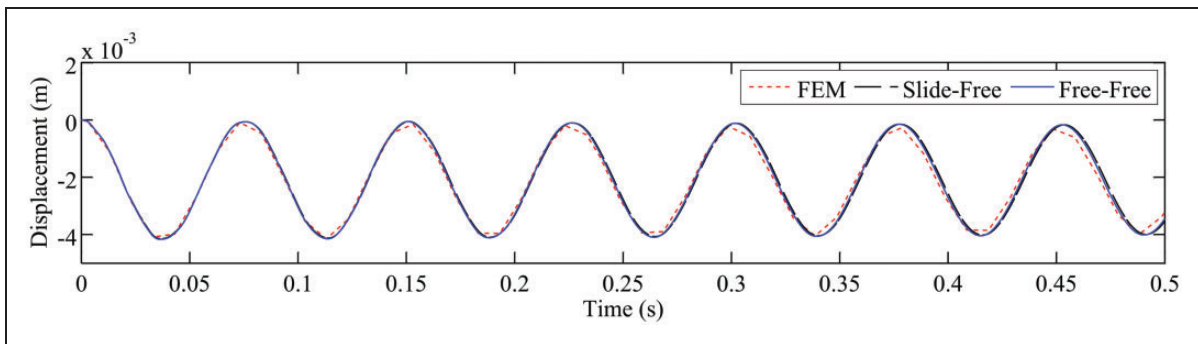


Figure 8. Case study I: elastic displacement of points A, B and C.

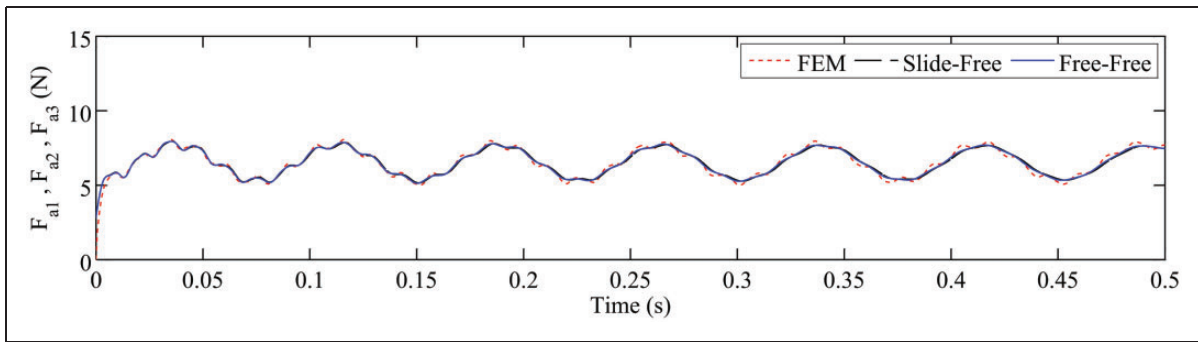


Figure 9. Case study I: amount of the three driving forces.

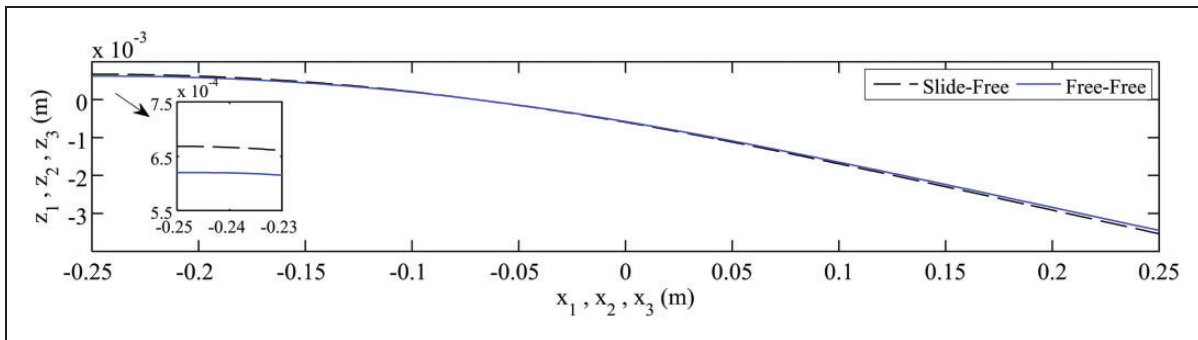


Figure 10. Case study I: beam shapes at  $t = 0.5$  s – deformation axis is magnified.

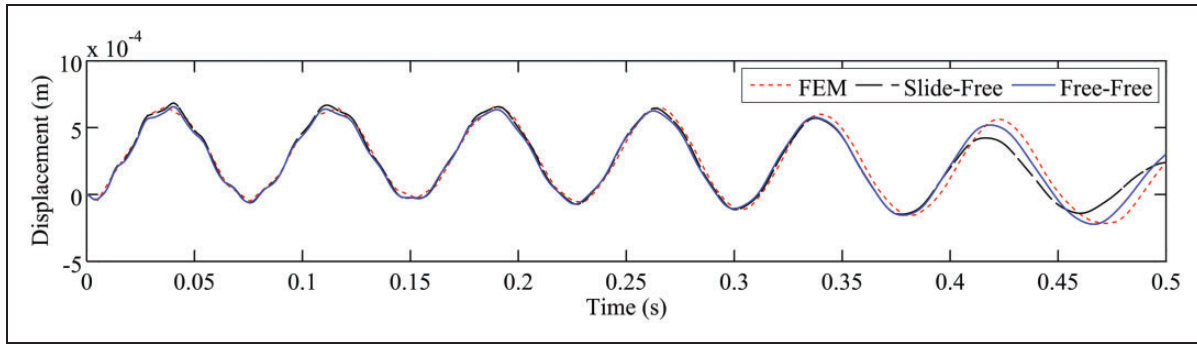


Figure 11. Case study 2: elastic displacement of point G.

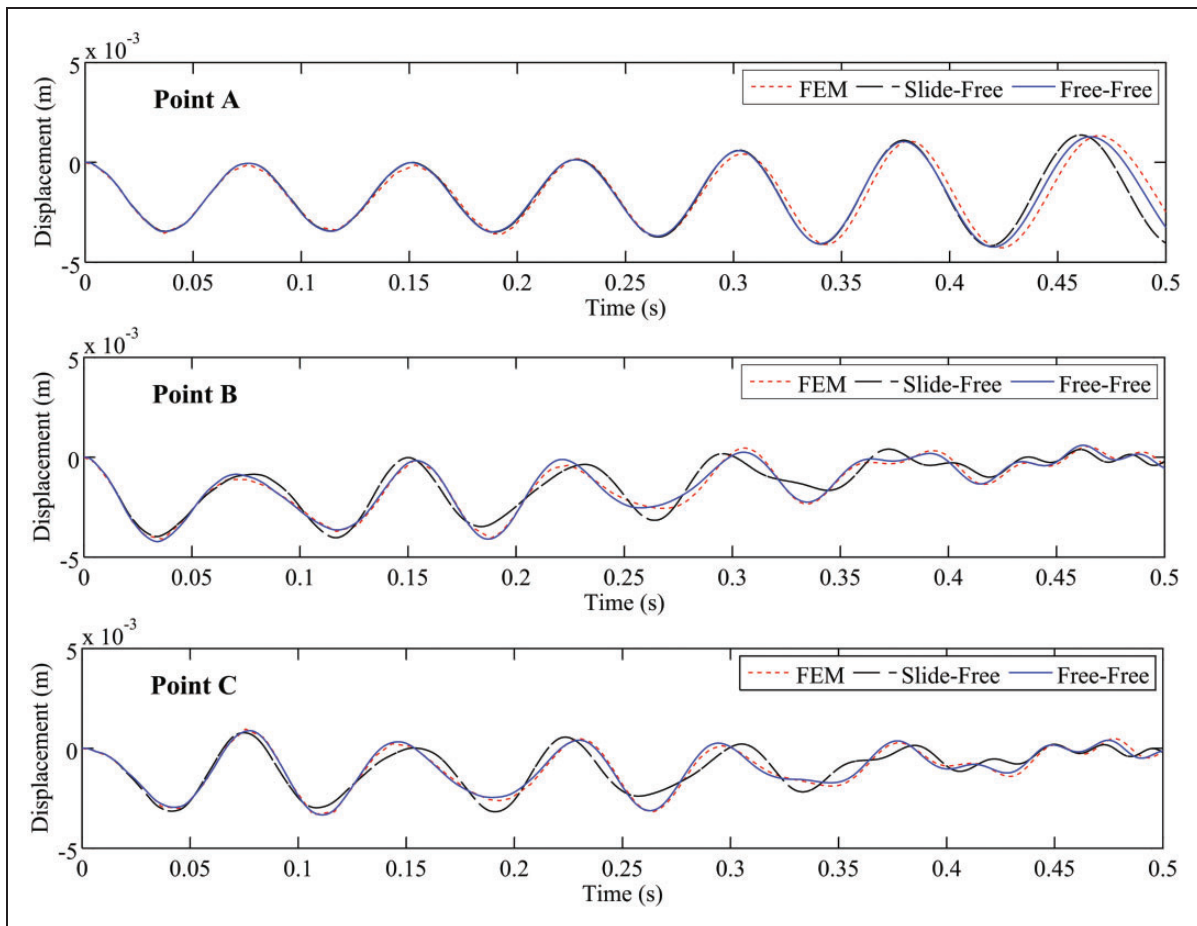
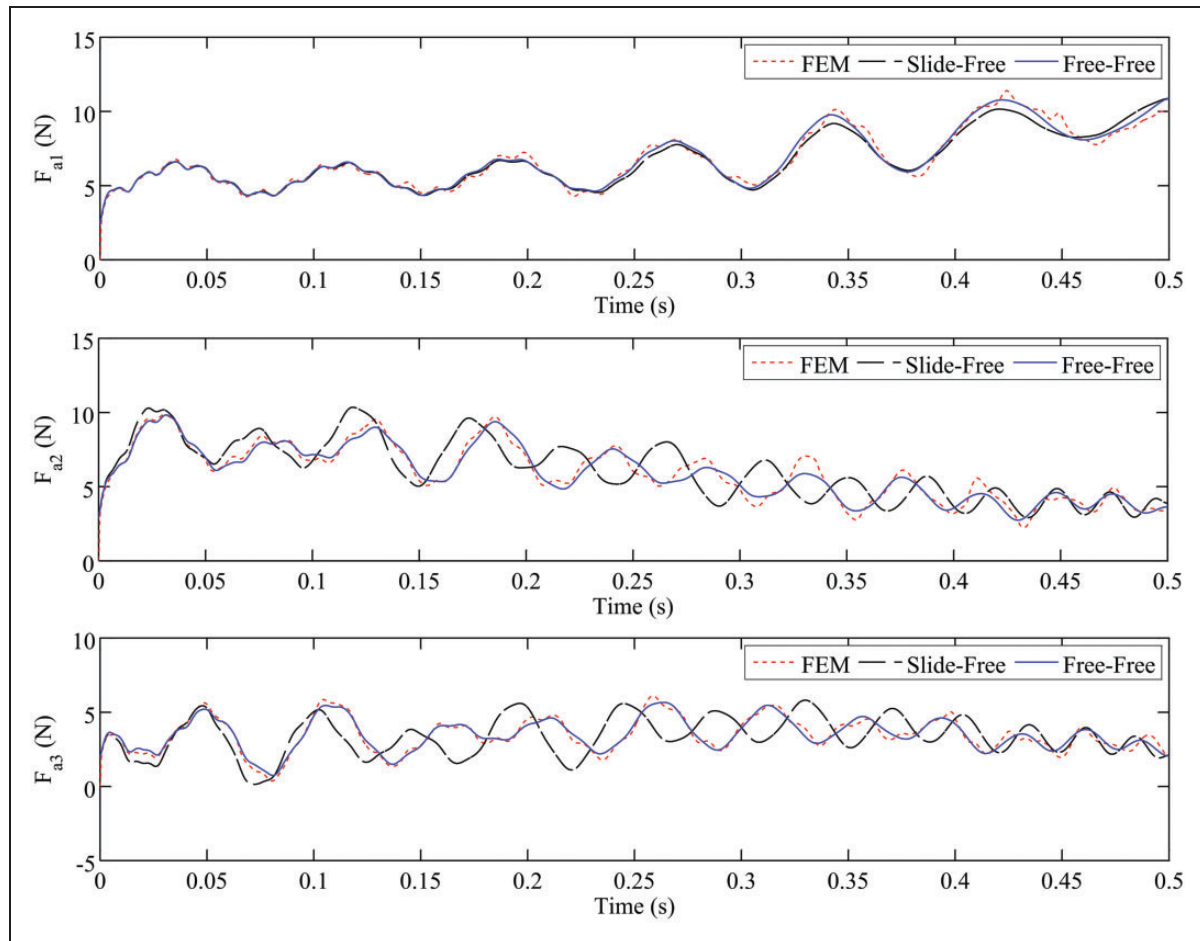


Figure 12. Case study 2: elastic displacement of points A, B and C.

of the elements in the FEM solution is 600. A spatial two-node linear beam element is used in the FEM solution. Let parameters  $a$  and  $b$  represent the thickness and width of each beam in the  $z_i$  and  $y_i$  directions, respectively. The physical properties of the 3-PSP robot are as  $a = 0.003(\text{m})$ ,  $b = 0.03(\text{m})$ ,  $E = 200 \times 10^9(\text{N/m}^2)$ ,  $I = 6.75 \times 10^{-11}(\text{m}^4)$ ,  $\rho = 0.702(\text{kg/m})$ ,  $d = 0.18(\text{m})$ ,

$L = 0.5(\text{m})$ ,  $L_p = 0.03(\text{m})$ ,  $m_p + m_s + m_l = 0.2(\text{kg})$  and  $I_{xx}^p = I_{yy}^p = I_{zz}^p = 2 \times 10^{-4}(\text{kg.m}^2)$ . The simulation time used in the three case studies is 0.5 seconds. The consumed CPU time for the approximate analytical method is approximately 10 minutes versus 65 minutes for the commercial FEM software.



**Figure 13.** Case study 2: amount of the three driving forces.

### 7.1. Case Study 1

For case study 1, the robot has a symmetric configuration and a rectilinear translation in the  $Z$ -direction. Additionally, the gravitational acceleration is in the  $Z$ -direction. The vibration of the working point of the robot, point  $G$ , is shown in Figure 7.

Additionally, vibration of the free ends of the beams, points  $A$ ,  $B$  and  $C$ , are considered. Figure 8 shows the elastic displacement for point  $A$ . In case study 1, transverse vibration of points  $B$  and  $C$  is identical to that of point  $A$  and therefore is not separately shown.

The amount of the three driving forces,  $F_{ai}$ , in case study 1 is shown in Figure 9. Because of the symmetrical motion, the values of all three driving forces are equal. Also note that, if the robot is assumed to be all rigid, then because of the symmetric configuration/motion and constant input acceleration, it is a simple task to calculate the necessary driving forces for case study 1 as  $F_{ai} = [3(m_p + m_s + m_l + \rho L)(\ddot{s}_i(t) + g)]/3 = 6.5018(N)$ . The three actuator forces remain constant during the motion. However, in the flexible case, as

shown in Figure 9, vibrational motion of the robot has a significant effect on the values of the driving forces.

As shown in Figures 6–8, for case study 1, analytical results and FEM results closely follow each other. Additionally, the accuracy of the responses obtained using the slide-free and free-free mode shapes are nearly identical. The deformed shape of the three beams of the star obtained at  $t = 0.5s$  using the slide-free and free-free mode shapes are shown in Figure 10. Note that  $x_i = -0.25$  represents the working point, point  $G'$ , where all three links are joined and the slope of all three beams becomes zero.

### 7.2. Case Study 2

In case study 2, the rigid star rotates about and translates along the  $y$ -axis. Additionally, the existence of the gravitational acceleration in the  $Z$ -direction acts as if the robot is moving in the  $Z$ -direction. Therefore, the moving star experiences a more general motion. Elastic displacement of point  $G$  is shown in Figure 11.

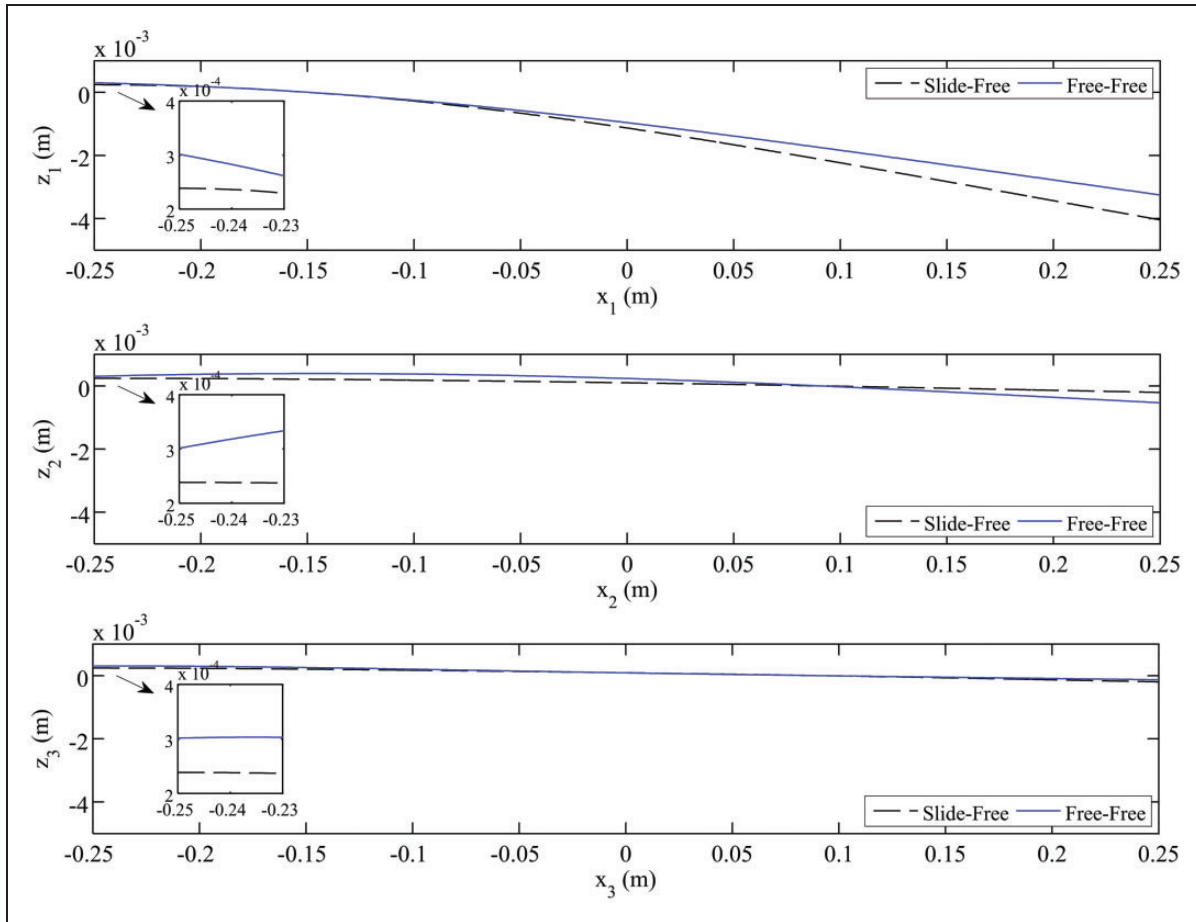


Figure 14. Case study 2: beam shapes at  $t = 0.5$  s – deformation axis is magnified.

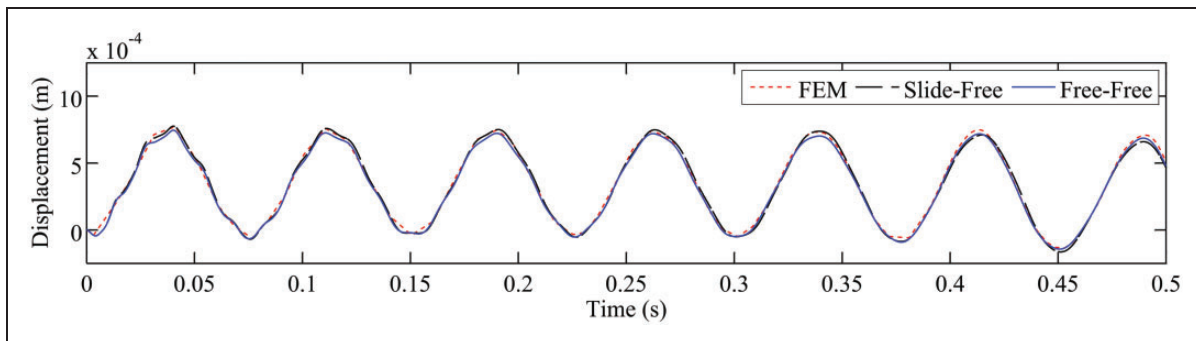


Figure 15. Case study 3: elastic displacement of the point G.

Next, elastic displacements for the free ends of the three beams, points  $A$ ,  $B$ , and  $C$ , are shown in Figure 12. For each of the points, the results of the free-free mode shapes are closer to the FEM results than the slide-free results.

The amount of the driving forces,  $F_{ai}$ , are shown in Figure 13. As can be seen from this figure, the

frequency of the responses obtained from the slide-free mode shapes is incorrect.

As shown in Figures 10–12, analytical results for the free-free mode shapes closely follow the FEM results. The accuracy of the responses obtained using the free-free mode shapes are significantly better than the slide-free case. This is due to that fact that the slide-free

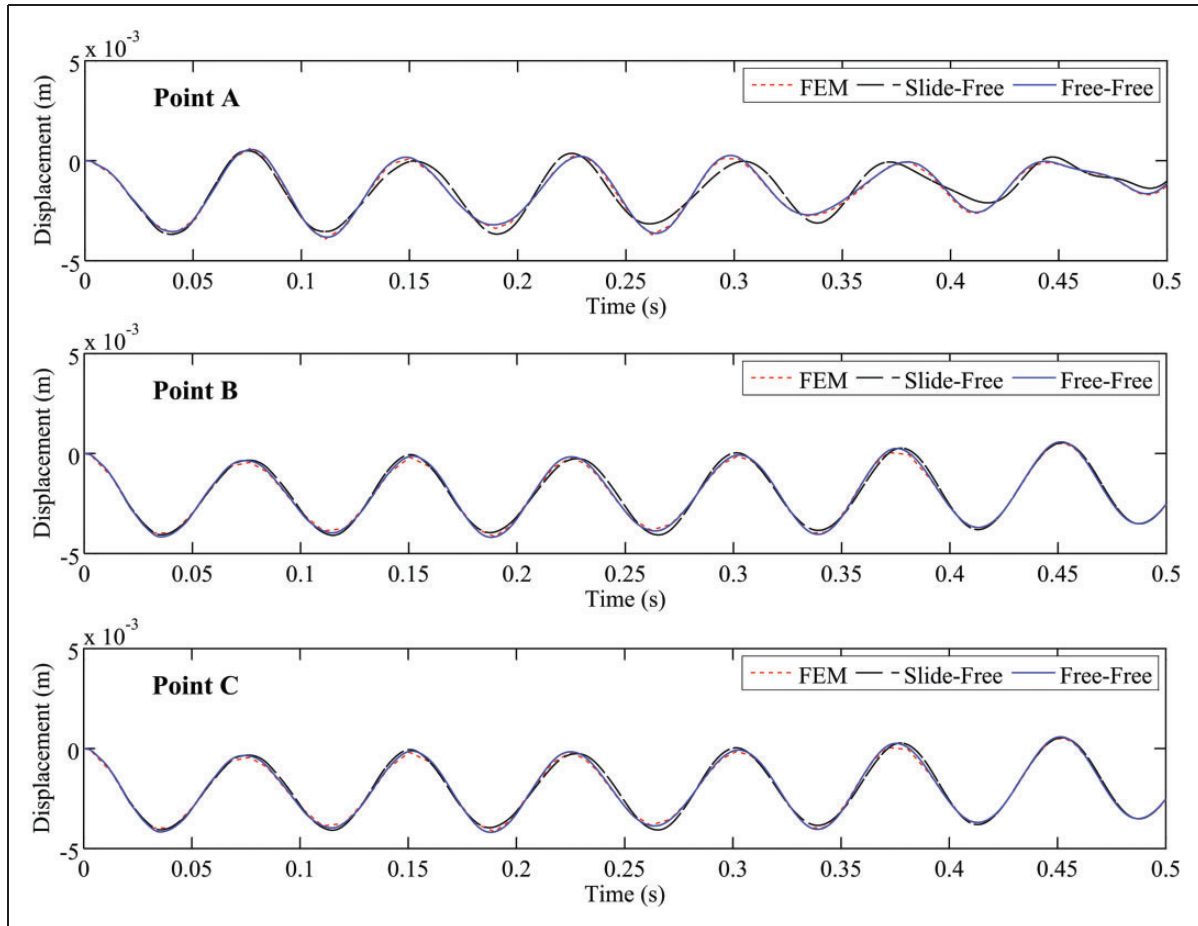


**Figure 16.** Case study 3: elastic displacement of points A, B and C.

mode shapes have the zero slope condition at their slide end and, therefore, incorrectly induce a zero slope condition at point *G*. Note that in case study 1, because of the symmetric motion of the star, the zero slope condition at point *G* was correct.

Finally, using the slide-free and free-free mode shapes, the deformed shape of the three beams of the star at  $t = 0.5$ s are obtained and shown in Figure 14. Note that due to unsymmetrical motion, the slope of the beams at point *G* is expected to be nonzero for the majority of the motion. Therefore, the choice of free-free mode shapes which do not force the slope of the beams at point *G* to be zero is correct.

### 7.3. Case Study 3

In case study 3, the input trajectories are set so that we have a symmetric motion with respect to the *YZ* plane (see Figure 2). The line *JK* translates along the *Z*-direction and rotates about the line *JK*. The gravitational acceleration is also in the *Z*-direction. This is a more general case study with respect to the case studies 1 and

2, which better illustrates the effect of the selected mode shapes on the accuracy of the vibrational responses. Elastic displacement of point *G* for case study 3 is shown in Figure 15.

Similar to the two previous case studies, elastic displacement for the free ends of the three beams, points *A*, *B*, and *C*, are also calculated and shown in Figure 16. Similar to case study 2, results obtained from the free-free mode shapes are more accurate than those of the slide-free mode shapes and more closely follow the FEM results. Because of the symmetric motion, elastic displacements of points *B* and *C* are identical.

The amount of the driving forces,  $F_{ai}$ , are calculated and shown in Figure 16. Results obtained from the free-free mode shapes are more accurate than those of the slide-free mode shapes. As shown in Figure 17, because of symmetric motion with respect to the *YZ* plane, the driving forces  $F_{a2}$  and  $F_{a3}$  are identical.

As shown in Figures 14–16, for case study 3 and similar to case study 2, the accuracy of the responses obtained using the free-free modes are more than

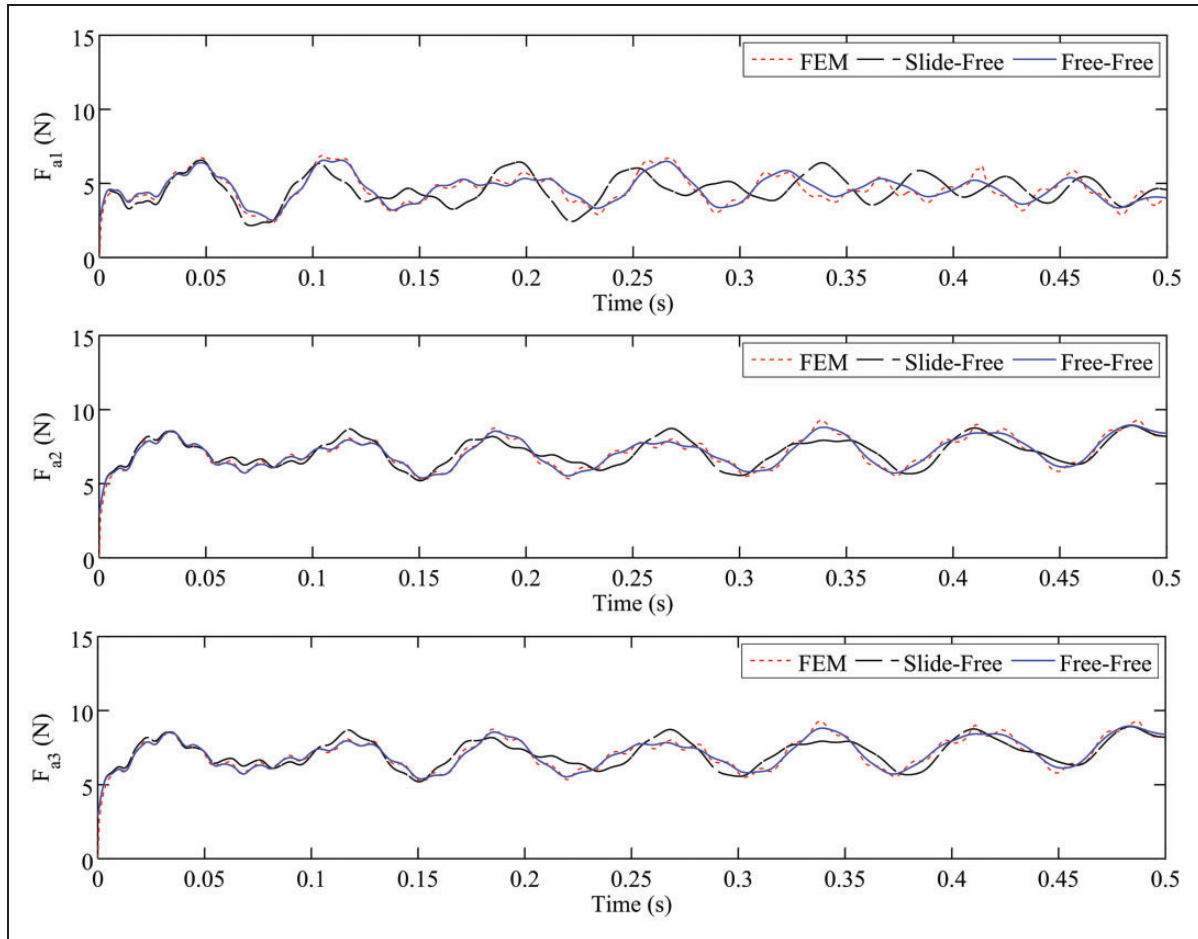


**Figure 17.** Case study 3: amount of the three driving forces.

the slide-free modes. Additionally, analytical results for the free-free mode shapes closely follow the FEM results. As mentioned earlier, the slide-free mode shapes incorrectly induce a zero slope condition at point  $G$  of the star which results in inaccurate responses.

The deformed shape of three beams of the moving platform obtained at  $t = 0.5$  s using the slide-free and free-free mode shapes are shown in Figure 18 for case study 3. Note that similar to unsymmetrical motion in case study 2, using the free-free modes the slope of all beams at point  $G$  is nonzero and the slide-free mode shapes cannot satisfy this boundary condition at point  $G$ .

## 8. Discussion on mode shape selection

The assumed mode method provides simplicity in solving vibrational motion equations. The traditional AMM typically requires some qualitative information about the geometrical conditions of the system motion,

i.e. geometrical boundary conditions. This information helps researchers to better select the type of assumed mode shapes. However, for certain points in some structures, the use of traditional boundary conditions for mode shapes may not be correct. In such cases, one solution is to use the mode shapes with free boundary conditions together with proper geometrical constraints. The free boundary conditions mean that geometrical boundary conditions are unspecified (free) and natural boundary conditions are specified (usually zero).

For example, in the case of the presented 3-PSP parallel robot with a moving platform made of three flexible beams, the point  $G$  does not have any specific geometrical boundary conditions. Therefore, use of modes with free geometrical conditions at point  $G$  together with the proper geometrical constraints resulted in obtaining the correct solution for the presented analytical model. On the other hand, using the slide geometrical conditions at point  $G$  resulted in an unacceptable solution.

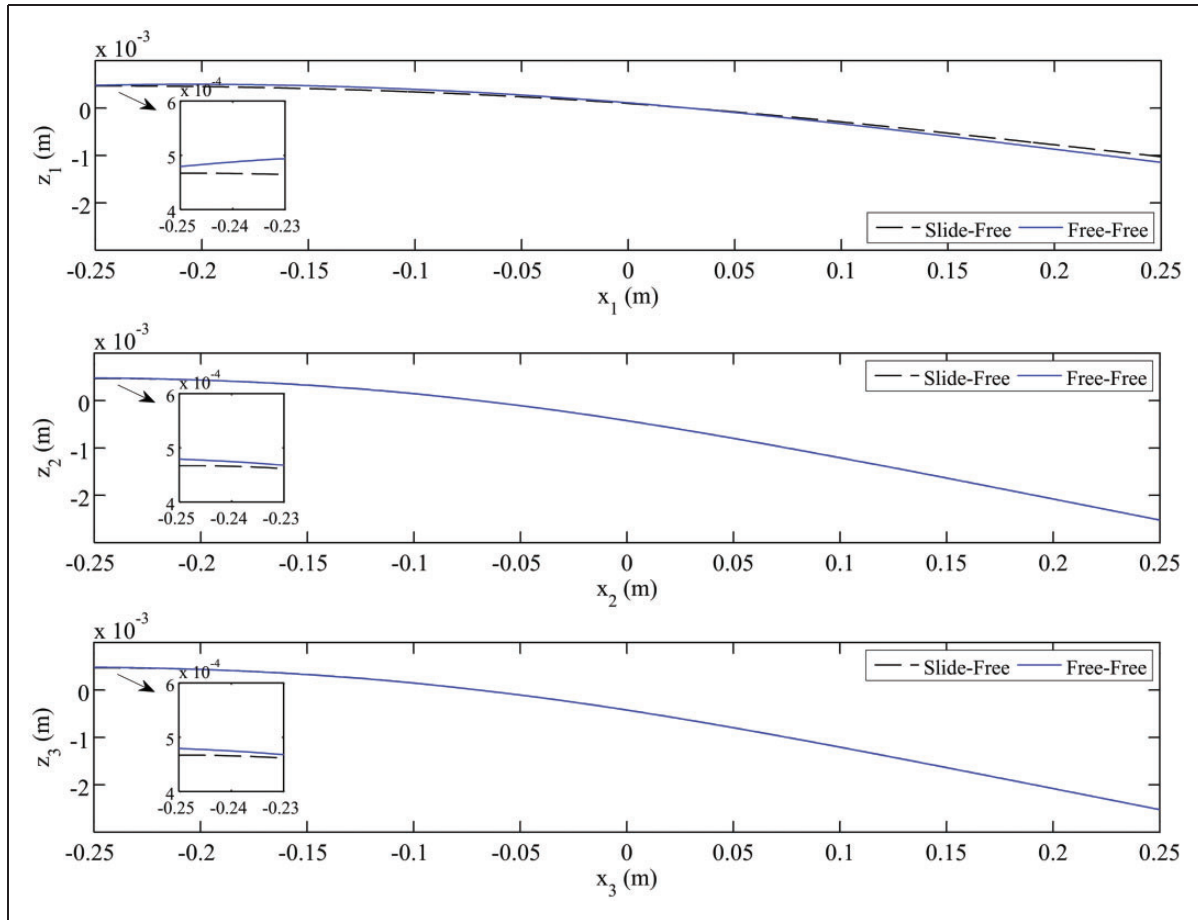


**Figure 18.** Case study 3: beam shapes at  $t = 0.5$  s – deformation axis is magnified.

## 9. Conclusion

In the present study, an analytical model and its approximate analytical solution were presented for dynamic and vibration analysis of a 3-PSP parallel robot with a flexible moving platform having three passive prismatic joints. In-plane bending stiffness for three beams of the moving star was assumed to be much higher than out-of-plane bending stiffness and consequently in-plane transverse vibration for the three beams was neglected. Direct kinematics was developed for acceleration analysis of the rigid robot. For dynamic modeling, the passive prismatic joints and junction point of the three flexible beams were modeled using a new set of geometric constraints. Additionally, a previously developed constrained motion equation for a planar Euler-Bernoulli beam having a prismatic joint was further developed for the three beams of the star. Next, an approximate analytical method was developed for solving the motion equations of the robot. To investigate the model's efficiency, three input trajectories and two

different groups of mode shapes were considered. Elastic displacements of free end points and the junction point of the three flexible beams of the star as well as the driving forces of the robot were compared with the FEM results. It was shown that accurate results were obtained using the free-free mode shapes and therefore the analytical model is correct.

The main contributions of this paper are: (1) Presenting an analytical model and its approximate analytical solution for dynamics and vibration of the 3-PSP parallel robot; (2) Obtaining the direct kinematics solution of the 3-PSP parallel robot; (3) Simultaneously solving the inverse/direct dynamics and vibration of the robot. Additional contributions of this paper are: (4) Presenting a new set of geometric constraints for dynamic modeling of the passive prismatic joints as well as presenting a new set of geometric constraints for the junction point of the three beams; (5) Investigating the effect of the selected assumed mode shapes on the accuracy of the approximate analytical solution.

## Funding

This research received no specific grant from any funding agency in the public, commercial, or not-for-profit sectors.

## References

- Banerjee AK and Kane TR (1987) Extrusion of a beam from a rotating base. *Journal of Guidance* 12(2): 140–149.
- Bauchau OA (2000) On the modeling of prismatic joints in flexible multi-body systems. *Computer Methods in Applied Mechanics and Engineering* 181: 87–105.
- Fattah A, Angeles J and Misra AK (1994a) Direct kinematics of a 3-DOF spatial parallel manipulator with flexible legs. In: *Proceedings of the ASME 23rd Biennial Conference on Mechanisms*, Minneapolis, USA, 11–14 September, vol. 72, pp. 285–291.
- Fattah A, Misra AK and Angeles J (1994b) Dynamics of a flexible-link planar parallel manipulator in Cartesian space. In: *Proceedings of the ASME 20th Conference on Design Automation*, Minneapolis, USA, 11–14 September, vol. 69(2), pp. 483–490.
- Fattah A, Angeles J and Misra AK (1995) Dynamics of a 3-DOF spatial parallel manipulator with flexible links. In: *Proceedings of the IEEE International Conference on Robotics and Automation*, Nagoya, Japan, 21–27 May, vol. 1, pp. 627–632.
- Gurgoze M and Yuksel S (1999) Transverse vibrations of a flexible beam sliding through a prismatic joint. *Journal of Sound and Vibration* 223(3): 467–482.
- Greenwood DT (2003) *Advanced Dynamics*, 1st edn. Cambridge: Cambridge University Press.
- Ibrahimbegovic A and Mamouri S (2000) On rigid components and joint constraints in nonlinear dynamics of flexible multibody systems employing 3D geometrically exact beam model. *Computer Methods in Applied Mechanics and Engineering* 188: 805–831.
- Kang B and Mills JK (2002) Dynamic modeling of structurally-flexible planar parallel manipulator. *Journal of Robotica* 20: 329–339.
- Krishnamurthy K (1989) Dynamic modeling of a flexible cylindrical manipulator. *Journal of Sound and Vibration* 132(1): 143–154.
- Lee U and Jang I (2007) On the boundary conditions for axially moving beams. *Journal of Sound and Vibration* 306: 675–690.
- Piras G, Cleghorn WL and Mills JK (2005) Dynamic finite-element analysis of a planar high-speed, high-precision parallel manipulator with flexible links. *Mechanism and Machine Theory* 40: 849–862.
- Rezaei A, Akbarzadeh A and Akbarzadeh-T M (2012) An investigation on stiffness of a 3-PSP spatial parallel mechanism with flexible moving platform using invariant form. *Journal of Mechanism and Machine Theory* 51: 195–216.
- Rezaei A, Akbarzadeh A, Mahmoodinia P and Akbarzadeh-T M (2013) Position, Jacobian and workspace analysis of a 3-PSP spatial parallel manipulator. *Journal of Robotics and Computer-Integrated Manufacturing* 29(4): 158–173.
- Shabana AA and Wehage RA (1983) Coordinate reduction technique for transient analysis of spatial substructures with large angular rotations. *Journal of Structural Mechanics* 11(3): 401–431.
- Sharifnia M and Akbarzadeh A (2014a) An analytical model for vibration and control of a PR-PRP parallel robot with flexible platform and prismatic joint. *Accepted in Journal of Vibration and Control* DOI: 10.1177/1077546314528966.
- Sharifnia M and Akbarzadeh A (2014b) Approximate analytical solution for vibration of a 3-PRP planar parallel robot with flexible moving platform. *Accepted in Journal of Robotica*. DOI: 10.1017/S0263574714001398.
- Song JO and Haug EJ (1980) Dynamic analysis of planar flexible mechanisms. *Computer Methods in Applied Mechanics and Engineering* 24(3): 359–381.
- Stoenescu ED and Marghitu DB (2004) Effect of prismatic joint inertia on dynamics of kinematic chains. *Mechanism and Machine Theory* 39: 431–443.
- Stylianou M and Tabarrok B (1994) Finite element analysis of an axially moving beam, Part I: Time integration. *Journal of Sound and Vibration* 178(4): 433–453.
- Sugiyama H, Escalona JL and Shabana AA (2003) Formulation of three-dimensional joint constraints using the absolute nodal coordinates. *Journal of Nonlinear Dynamics* 31: 167–195.
- Tabarrok B, Leech CM and Kim YI (1974) On the dynamics of an axially moving beam. *Journal of the Franklin Institute* 297(3): 201–220.
- Theodore RJ and Ghosal A (1997) Modeling of flexible-link manipulators with prismatic joints. *IEEE Transactions on Systems, Man, and Cybernetics—Part B: Cybernetics* 27(2): 296–305.
- Wang PKC and Wei JD (1987) Vibrations in a moving flexible robot arm. *Journal of Sound and Vibration* 116(1): 149–160.
- Wang X and Mills JK (2006) Dynamic modeling of a flexible-link planar parallel platform using a substructuring approach. *Mechanism and Machine Theory* 41: 671–687.
- Yoo WS and Haug EJ (1986a) Dynamics of flexible mechanical systems using vibration and static correction modes. *Journal of Mechanisms, Transmissions and Automation in Design* 108(3): 315–322.
- Yoo WS and Haug EJ (1986b) Dynamics of articulated structures. Part I. Theory. *Journal of Structural Mechanics* 14(1): 105–126.
- Yuh J, Young T and Beak YS (1989) Modeling of a flexible link having a prismatic joint in robot mechanism – experimental verification. In: *Proceeding of the IEEE International Conference on Robotics and Automation*, Scottsdale, AZ, 14–19 May, vol. 2, pp. 722–727.
- Zhang X, Mills JK and Cleghorn WL (2008) Vibration control of elastodynamic response of a 3-PRR flexible parallel manipulator using PZT transducers. *Journal of Robotica* 26: 655–665.